Appl. Math. Mech. -Engl. Ed., **42**(2), 183–208 (2021)

APPLIED MATHEMATICS AND MECHANICS (ENGLISH EDITION)

https://doi.org/10.1007/s10483-021-2673-9

Analytical solution for the stress field of hierarchical defects: multiscale framework and applications*

Baijian WU[1,2], Sheng ZHOU[1,2], Zhaoxia LI[1,2,†]

1. Jiangsu Key Laboratory of Engineering Mechanics, Southeast University, Nanjing 210096, China;
2. Department of Engineering Mechanics, Southeast University, Nanjing 210096, China

(Received May 3, 2020 / Revised Jul. 6, 2020)

Abstract Hierarchical defects are defined as adjacent defects at different length scales. Involved are the two scales where the stress field distribution is interrelated. Based on the complex variable method and conformal mapping, a multiscale framework for solving the problems of hierarchical defects is formulated. The separated representations of mapping function, the governing equations of potentials, and the stress field are subsequently obtained. The proposed multiscale framework can be used to solve a variety of simplified engineering problems. The case in point is the analytical solution of a macroscopic elliptic hole with a microscopic circular edge defect. The results indicate that the microscopic defect aggregates the stress concentration on the macroscopic defect and likely leads to global propagation and rupture. Multiple micro-defects have interactive effects on the distribution of the stress field. The level of stress concentration may be reduced by the coalescence of micro-defects. This work provides a unified method to analytically investigate the influence of edge micro-defects within the scope of multiscale hierarchy. The formulated multiscale approach can also be potentially applied to materials with hierarchical defects, such as additive manufacturing and bio-inspired materials.

Key words hierarchical defect, stress field, multiscale framework, scale separation, complex variable method, elliptic crack, edge defect

Chinese Library Classification O302, O343
2010 Mathematics Subject Classification 35Q74, 74S70, 74G10

Nomenclature

E,	Young's modulus;	ψ,	complex potential;
ν,	Poisson's ratio;	ω,	conformal transformation;
σ,	stress;	K,	stress concentration factor (SCF);
u,	displacement;	r,	defect size in z-plane;
φ,	complex potential;	ρ,	defect size in ζ-plane;

* Citation: WU, B. J., ZHOU, S., and LI, Z. X. Analytical solution for the stress field of hierarchical defects: multiscale framework and applications. *Applied Mathematics and Mechanics* (*English Edition*), **42**(2), 183–208 (2021) https://doi.org/10.1007/s10483-021-2673-9

† Corresponding author, E-mail: zhxli@seu.edu.cn

Project supported by the National Natural Science Foundation of China (No. 51878154) and the National Program on Major Research Project of China (No. 2016YFC0701301)

Ω, domain in z-plane; Γ, unit circle.
D, unit disk in ζ-plane;

1 Introduction

During the manufacturing process, microscopic edge defects emerge around non-ideal cracks such as elliptic cracks and inclusion. The adjacent defects at different length scales can be described as hierarchical defects. Usually, there are two scales involved. Presence of the microscopic defect has substantial influence over the stress level at the macroscopic defect, and possibly leads to global crack propagation and rupture[1–2]. The effects of the microscopic defect on the macroscopic crack propagation cannot be over-emphasized. Seeking the solution of the stress field at the crack tip is of great significance to engineering practice.

For non-ideal cracks, calculation of the stress field at the crack tip is relatively complex[3–4]. Analytical solutions and numerical methods stand out as the two main approaches. Pioneering research work includes the Westergaard stress function, the integral equation method, and the complex variable method[5–6]. These analytical solutions play an important role in the early stage of fracture mechanics. With the development of computational technique, numerical methods emerged, such as the finite element method[7–8] and the boundary element technique[9–10]. Through commercial softwares, the discretization method is generally adopted to approximately calculate the stress field distribution at the crack tip. Considering the complexity and variety of cracks, formulating a universal representation of the stress field at the crack tip is almost impossible. Tremendous calculation is needed, and the major effect factors are difficult to be extracted through the numerical methods. On the contrary, the major factors can be straightforwardly reflected in the analytical solutions. Although certain limitations cannot be avoided, accurate analytical solutions for the stress field at the crack tip remain prevalent yet more challenging among modern researchers.

A series of studies are initiated to seek the analytical solutions of notches and cracks[11–13]. Based on the analytical framework, the notch stress intensity factor (NSIF) is applied to the weld roots of welded joints with inclusion of the T-stress component[14]. It is noteworthy that the T-stress is determined from the finite element models evaluating the ligament stresses close to the pointed slit tip. Similar work can be found in Refs. [15] and [16]. Much progress has also been made to analytically solve the problem of edge dislocation in front of blunt crack for nanocrystalline materials[17–19]. Recent work witnesses that the use of digital image correlation method is combined with analytical analysis for determining the stress field at blunt V-notch neighborhood[20–21]. Despite the accumulating research on the analytical approach, it shall be emphasized that the multiscaling features of hierarchal defects are rarely addressed recently. A series of studies[16, 22–23] incorporated the multiscaling features in the crack growth model. Analytical representation of the stress intensity factor is derived for macroscopic crack possessing a micro/mesoscopic notch tip. The concept is further applied to the fatigue crack growth model[24–26]. Nevertheless, the model is stipulated to ideal cracks that are different from the hierarchical defects described here. To the best of the authors' knowledge, the research on the analytical solution for hierarchical defects is rather surprising within the framework of multiscaling.

The aim of this paper is to formulate a multiscale framework for the analytical stress field solution of hierarchical defects. The strategy is to employ the scale separation method, as well as the conformal mapping of complex variable method. Therefore, the analytical solution for the stress field at the crack tip is obtained. The present work focuses on the hierarchical defects where two scales are involved through the process. Subsequently, the proposed framework is applied to analytically investigate a macroscopic elliptic crack with microscopic circular edge defects. The framework is flexible to solve a variety of simplified engineering problems.

The general multiscale framework is formulated in Section 2, which is mainly based on the

complex variable method and the scale separation method. The applications of the proposed framework are presented in Sections 3 and 4, with the emphasis put on single and multiple edge defects at the microscopic scale. Conclusions are briefly summarized in Section 5.

2 Complex variable method for solving the stress field of hierarchical defects: a multiscale framework

2.1 Basic formulation of the complex variable method

According to the complex variable method[5], the stress and displacement of an elastic continuum can be expressed in the form of functions of complex variables when the body force is ignored, which yields

$$\begin{cases} \sigma_x + \sigma_y = 2(\varphi_1'(z) + \overline{\varphi_1'(z)}) = 4\,\mathrm{Re}\,\varphi_1'(z), \\ \sigma_y - \sigma_x + 2\mathrm{i}\,\tau_{xy} = 2(\overline{z}\varphi_1''(z) + \psi_1'(z)), \end{cases} \tag{1}$$

$$\frac{E}{1-\nu}(u_x + \mathrm{i}\,u_y) = \frac{3-\nu}{1+\nu}\varphi_1(z) - z\overline{\varphi_1'(z)} - \overline{\psi_1(z)}, \tag{2}$$

where E and ν are Young's modulus and Poisson's ratio of the material, respectively. $\varphi_1(z)$ and $\psi_1(z)$ are called the complex potentials which are both analytic or holomorphic functions inside the domain of Ω. Since the analytic function is equivalent to the holomorphic function in complex analysis, in what follows, these two terms are interchangeably used.

For the hole problems, technique of conformal mapping is jointly used with the above theory. If a transformation that could map the actual domain Ω (usually an infinite plane containing a hole/defect in the z-plane $z = x + \mathrm{i}y$) onto a unit disk D in the ζ-plane ($\zeta = \xi + \mathrm{i}\eta$) is found as follows:

$$z = \omega(\zeta), \tag{3}$$

the complex potentials are in the forms of

$$\varphi(\zeta) = \frac{1-\nu}{8\pi}(X + \mathrm{i}\,Y)\ln\zeta + B\omega(\zeta) + \varphi_0(\zeta),$$

$$\psi(\zeta) = \frac{3-\nu}{8\pi}(X - \mathrm{i}\,Y)\ln\zeta + (B' + \mathrm{i}C')\omega(\zeta) + \psi_0(\zeta),$$

where $\varphi(\zeta) = \varphi_1\big(\omega(\zeta)\big)$ and $\psi(\zeta) = \psi_1\big(\omega(\zeta)\big)$ are both analytic functions in the open unit disk, and are determined by the boundary conditions. The complex number $X + \mathrm{i}Y$ is related to the boundary force applied on the inner hole. If the inner forces do not exist, the above equations could be simplified as

$$\begin{cases} \varphi(\zeta) = B\omega(\zeta) + \varphi_0(\zeta), \\ \psi(\zeta) = (B' + \mathrm{i}\,C')\omega(\zeta) + \psi_0(\zeta). \end{cases} \tag{4}$$

Furthermore, $\varphi_0(\zeta)$ and $\psi_0(\zeta)$ are governed by the following integral equations:

$$\begin{cases} \varphi_0(\zeta) + \dfrac{1}{2\pi\mathrm{i}}\displaystyle\int_\Gamma \frac{\omega(\sigma)}{\overline{\omega'(\sigma)}}\frac{\overline{\varphi_0'(\sigma)}}{\sigma-\zeta}\mathrm{d}\sigma = \frac{1}{2\pi\mathrm{i}}\int_\Gamma \frac{f_0}{\sigma-\zeta}\mathrm{d}\sigma, \\ \psi_0(\zeta) + \dfrac{1}{2\pi\mathrm{i}}\displaystyle\int_\Gamma \frac{\overline{\omega(\sigma)}}{\omega'(\sigma)}\frac{\varphi_0'(\sigma)}{\sigma-\zeta}\mathrm{d}\sigma = \frac{1}{2\pi\mathrm{i}}\int_\Gamma \frac{\overline{f_0}}{\sigma-\zeta}\mathrm{d}\sigma, \end{cases} \tag{5}$$

where Γ is the unit circle, and $\sigma = \zeta|_\Gamma = \mathrm{e}^{\mathrm{i}\theta}$, denoting that ζ is now on the boundary Γ. Also, we have

$$f_0 = -2B\omega(\sigma) - (B' - \mathrm{i}\,C')\overline{\omega(\sigma)}, \tag{6}$$

where B and $B'-\mathrm{i}\,C'$ are determined by the remote stress status, corresponding to hydrostatic and shearing stress, respectively,

$$B=\frac{1}{4}(\sigma_1+\sigma_2),\quad B'+\mathrm{i}C'=-\frac{1}{2}(\sigma_1-\sigma_2)\mathrm{e}^{-2\mathrm{i}\gamma}, \tag{7}$$

in which γ is the included angle between the first principal stress σ_1 and the x-axis. In the condition of remotely uniaxial tension, assuming that the tensile stress q is applied in the direction of γ, the above equations could be further simplified as

$$\begin{cases}\varphi(\zeta)=\dfrac{q}{4}\omega(\zeta)+\varphi_0(\zeta),\\ \psi(\zeta)=-\dfrac{q}{2}\mathrm{e}^{-2\mathrm{i}\gamma}\omega(\zeta)+\psi_0(\zeta),\end{cases} \tag{8}$$

$$f_0=-\frac{q}{2}\omega(\sigma)+\frac{q}{2}\overline{\omega(\sigma)}\mathrm{e}^{2\mathrm{i}\gamma}. \tag{9}$$

Then, denote

$$\Phi(\zeta)=\varphi_1'(z)=\frac{\varphi'(\zeta)}{\omega'(\zeta)},\quad \Psi(\zeta)=\psi_1'(z)=\frac{\psi'(\zeta)}{\omega'(\zeta)}. \tag{10}$$

The stress components described on the mapped curvilinear coordinates could be further written as[5]

$$\begin{cases}\sigma_\theta+\sigma_\rho=4\mathrm{Re}\dfrac{\varphi'(\zeta)}{\omega'(\zeta)}=4\mathrm{Re}\Phi(\zeta),\\ \sigma_\theta-\sigma_\rho+2\mathrm{i}\tau_{\rho\theta}=\dfrac{2\zeta}{\overline{\zeta}\omega'(\zeta)}(\overline{\omega(\zeta)}\Phi'(\zeta)+\omega'(\zeta)\Psi(\zeta)),\end{cases} \tag{11}$$

where ρ and θ are the directions mapped from the ξ-axis and the η-axis, respectively.

2.2 Conformal mapping and scale separation for problems of hierarchical defects

In this section, we start from a normalized case and further generalize the problem. Finally, the universal form of separated mapping functions at multiple scales is derived.

First, we consider an infinite plate with a circular hole and a semicircular micro-defect on its edge (specifically at $z=1$), as shown in Fig. 1(a). The function, which transforms the unit disk (the ζ-plane) into an infinite plane with a unit circular hole (the z_1-plane), can be expressed as

$$\omega_0(\zeta)=\frac{1}{\zeta}. \tag{12}$$

Assume that the analytic function of complex variable mapping the hierarchical-defects domain (see Fig. 1(a) in the z-plane) onto the unit disk (see Fig. 1(b) in the ζ-plane) has been found as $z=\omega(\zeta)$. Then, the deviation from the original mapping function ω_0 could be defined as

$$\delta(\zeta)=\omega-\omega_0=\omega(\zeta)-\frac{1}{\zeta}. \tag{13}$$

Generally, $\delta(\zeta)$ maps the unit disk to a very small defect in the order of $\rho\ll 1$, as shown in Fig. 1(c). The $\delta(\zeta)$ function, which though may have branch points on the boundary of $|\zeta|=1$, is holomorphic inside the open unit disk. Similar to a compactly supported function, its value falls in the order of ρ in the very neighborhood of the micro-defect (i.e., $\zeta=1$ here), and dramatically approaches zero when ζ is far from the defect. Detailed discussion on this function could be found in Subsection 3.1. It should be noted that this paper just illustrates an example where the microscopic edge defect is modeled as a semicircular hole. In fact, the micro-defect could be a crack or other shapes in the multiscale framework.

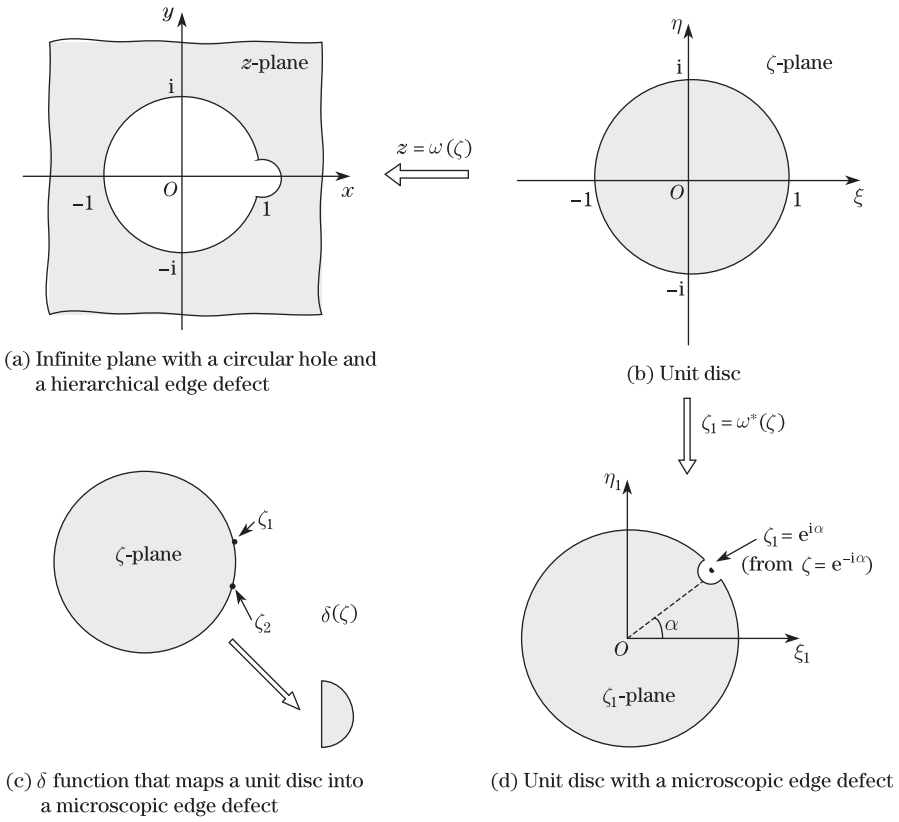

(a) Infinite plane with a circular hole and a hierarchical edge defect

(b) Unit disc

(c) δ function that maps a unit disc into a microscopic edge defect

(d) Unit disc with a microscopic edge defect

Fig. 1 Conformal mapping

$\delta(\zeta)$ could be modified to embed the possibility of randomly distributed micro-defects. In order to locate the defect at $z = \mathrm{e}^{\mathrm{i}\alpha}$, the function could be constructed as

$$\delta(\zeta, \alpha) = \mathrm{e}^{\mathrm{i}\,\alpha}\omega(\mathrm{e}^{\mathrm{i}\,\alpha}\zeta) - \frac{1}{\zeta}. \tag{14}$$

Then, Eq. (14) could transform $\zeta = \mathrm{e}^{-\mathrm{i}\alpha}$ to a micro-defect. Now, a new mapping function $\omega^*(\zeta, \alpha)$ that maps an ideal unit disk (the ζ-plane) to the micro-defected unit disk on its edge (here described in the ζ_1-plane), as shown in Fig. 1(d), could be constructed by combining Eqs. (13) and (14),

$$\zeta_1 = \omega^*(\zeta) = \frac{1}{\mathrm{e}^{\mathrm{i}\,\alpha}\omega(\mathrm{e}^{\mathrm{i}\,\alpha}\zeta)} = \frac{1}{1/\zeta + \delta(\zeta, \alpha)}. \tag{15}$$

From Eq. (15), a general form of conformal mapping that treats the arbitrary shape of hole could be derived. Assuming that the original function which maps the unit disk onto an infinite plate with this hole (without any edge defect) is known,

$$z_0 = \omega_0(\zeta) = \sum_{n=-1}^{\infty} c_n \zeta^n, \tag{16}$$

where c_n are complex constants. Substituting the variable ζ_1 in Eq. (15) into ζ in Eq. (16), the required function $\omega(\zeta)$ is obtained. It could successfully map the unit disk to an infinite

plate containing a general hole (the primary defect) as well as a microscopic edge defect (the secondary defect).

$$z = \omega(\zeta) = \omega_0(\zeta_1) = \omega_0\Big(\frac{1}{1/\zeta + \delta(\zeta, \alpha)}\Big). \tag{17}$$

Figures 2(a) and 2(b) show two cases of elliptic and square holes, respectively, using Eq. (17), where the original mapping functions $\omega_0(\zeta)$ could be found in Ref. [5].

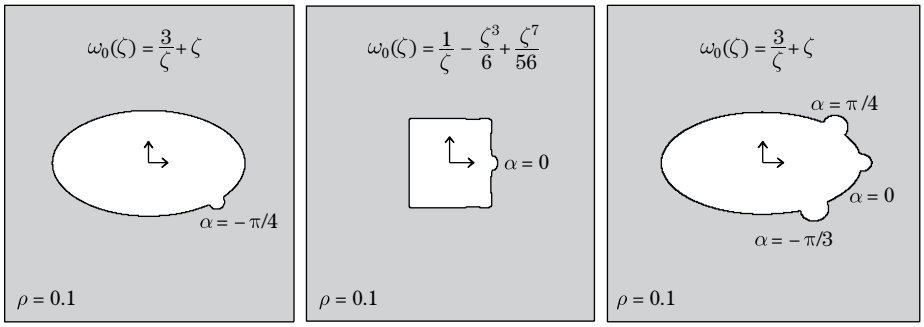

(a) (b) (c)

Fig. 2 Conformal mapping for arbitrary shapes of holes

Since the value of $\delta(\zeta, \alpha)$ is far less than 1, the mapping function of Eq. (15) could be asymptotically expanded as follows:

$$\Big(\frac{1}{1/\zeta\ + \delta(\zeta, \alpha)}\Big)^n = \zeta^n - n\zeta^{n+1}\delta(\zeta, \alpha) + O(\delta^2).$$

Ignoring higher-order terms over $O(\delta)$, Eq. (17) turns out to be

$$\begin{aligned} z = \omega(\zeta) = \omega_0(\zeta_1) &= \sum_{n=-1}^{\infty} c_n\Big(\frac{1}{1/\zeta\ + \delta(\zeta, \alpha)}\Big)^n = \sum_{n=-1}^{\infty} c_n(\zeta^n - n\zeta^{n+1}\delta(\zeta, \alpha)) \\ &= \sum_{n=-1}^{\infty} c_n\zeta^n - \zeta^2\delta(\zeta, \alpha)\sum_{n=-1}^{\infty} c_n n\zeta^{n-1} \\ &= \omega_0(\zeta) - \zeta^2\omega_0'(\zeta)\delta(\zeta, \alpha). \end{aligned}$$

It is noticed that $\delta(\zeta)$ is a compactly supported function when ζ is far from $\mathrm{e}^{-\mathrm{i}\alpha}$, $\delta(\zeta)$ approaches zero rapidly. The above equation could also be written as

$$\omega(\zeta) = \omega_0(\zeta) - \zeta^2\omega_0'(\zeta)\delta(\zeta, \alpha) \approx \omega_0(\zeta) - \mathrm{e}^{-2\mathrm{i}\alpha}\omega_0'(\mathrm{e}^{-\mathrm{i}\alpha})\delta(\zeta, \alpha). \tag{18}$$

Obviously, $\zeta^2\omega_0'(\zeta) \neq 0$ on the contour $|\zeta| = 1$.

Equation (18) is the asymptotic form that transforms a unit disk in the ζ-plane onto the plate with an arbitrary shape of the hole and a microscopic edge defect. To be specific, the location of the micro-defect is at $\zeta = \mathrm{e}^{-\mathrm{i}\alpha}$ in the ζ-plane, $\zeta_1 = \mathrm{e}^{\mathrm{i}\alpha}$ in the ζ_1-plane, and/or $z = \omega_0(\mathrm{e}^{-\mathrm{i}\alpha})$ in the z-plane.

Defining that

$$k = -\mathrm{e}^{-2\mathrm{i}\alpha}\omega_0'(\mathrm{e}^{-\mathrm{i}\alpha}), \tag{19}$$

Eq. (18) could be rewritten as

$$\omega(\zeta) = \omega_0(\zeta_1) \approx \omega_0(\zeta) + k\delta(\zeta, \alpha), \tag{20}$$

or more directly, be written in the scale separated form as

$$\omega(\zeta) = \omega_{\text{macro}}(\zeta) + \omega_{\text{micro}}(\zeta). \tag{21}$$

Here, ω_{macro} is ω_0, and $\omega_{\text{micro}} = k\delta(\zeta)$. To facilitate formula writing, the notation of ω_0 would be kept later.

In Eq. (20), the first term is the mapping function for the primary defect (the hole), and the second term is the perturbation due to the existence of the secondary defect (the microscale edge defect). The parameter k defined in Eq. (19) is a scaling factor for micro-defect due to the transformation process, which is related to $\omega_0(\zeta)$, the defect location, and the defect size.

2.3 Governing equations at separated scales

Starting from Eq. (4), we try to separate $\varphi_{\text{micro}}(\zeta)$ from $\varphi(\zeta)$, as well as $\psi_{\text{micro}}(\zeta)$ from $\psi(\zeta)$.

$$\varphi(\zeta) = \varphi_{\text{macro}}(\zeta) + \varphi_{\text{micro}}(\zeta), \quad \psi(\zeta) = \psi_{\text{macro}}(\zeta) + \psi_{\text{micro}}(\zeta). \tag{22}$$

It is found from Eq. (4) that the complex variables of B and $B' + \mathrm{i}\,C'$ are both scale independent. Since the mapping function $\omega(\zeta)$ has been written in a separated form as shown in Eq. (20) or (21), we now focus on separating $\varphi_{0,\text{micro}}$ and $\psi_{0,\text{micro}}$ in Eq. (5), i.e.,

$$\varphi_0 = \varphi_{0,\text{macro}}(\zeta) + \varphi_{0,\text{micro}}(\zeta), \quad \psi_0 = \psi_{0,\text{macro}}(\zeta) + \psi_{0,\text{micro}}(\zeta). \tag{23}$$

First of all, f_0 in the right-side integral of Eq. (5) could be simply divided into two parts. According to Eqs. (6) and (7), we have

$$f_0 = f_{0,\text{macro}} + f_{0,\text{micro}}, \tag{24}$$

where

$$\begin{cases} f_{0,\text{macro}} = -2B\omega_0(\sigma) - (B' - \mathrm{i}C')\overline{\omega_0(\sigma)}, \\ f_{0,\text{micro}} = -2B\omega_{\text{micro}}(\sigma) - (B' - \mathrm{i}C')\overline{\omega_{\text{micro}}(\sigma)}. \end{cases} \tag{25}$$

Now, we focus on the integral on the left side of Eq. (5),

$$\frac{1}{2\pi\mathrm{i}} \int_\Gamma \frac{\omega(\sigma)}{\overline{\omega'(\sigma)}} \frac{\overline{\varphi_0'(\sigma)}}{\sigma - \zeta} \mathrm{d}\sigma.$$

According to Eq. (17), the derivative of $\omega(\zeta)$ could be written as

$$\omega'(\zeta) = \omega_0'(\zeta_1) \frac{\mathrm{d}\zeta_1}{\mathrm{d}\zeta}. \tag{26}$$

Since $\omega_0(\zeta)$ and $\omega^*(\zeta)$ are both conformal transformations that are reversible and single-valued, $\omega_0'(\zeta)$ has no zeros inside the open unit disk $|\zeta| < 1$, which also applies to $\mathrm{d}\zeta_1/\mathrm{d}\zeta$. It should be noted that in some cases, the derivative may equal zero on the boundary Γ. A typical example is a crack, where one geometric point on the crack surface may correspond to two material points. At this time, $\omega_0'(\zeta) = 0$ occurs at the crack tip (the z-plane), corresponding to one certain point on the boundary of $|\zeta| = 1$ in the ζ-plane. Overall, there is no zero point inside the unit circle for $\omega'(\zeta)$.

As for poles, $\omega_0(\zeta)$ is holomorphic inside the unit domain except 0. At $\zeta = 0$, $\omega_0(\zeta)$ has order 1 singularity. Therefore, $\omega_0'(\zeta)$ has only one pole of order 2 at 0 in $|\zeta| < 1$. In the case of $\zeta_1(0) = 0$ which could be satisfied during the construction of $\delta(\zeta)$ function, $\zeta = 0$ also becomes the pole in order 2 for $\omega'(\zeta)$.

Considering σ on the boundary Γ, we have $\overline{\sigma}=1/\sigma$ and

$$\frac{\omega(\sigma)}{\overline{\omega'}(1/\sigma)}=\frac{\sigma^2\omega(\sigma)}{\overline{\omega'}(\sigma)}.$$

Since $\omega'(\sigma)$ has no zeros and $\sigma^2\omega(\sigma)$ is bounded, the above expression is analytic in the open disk, and thus could be written in the form of Taylor series,

$$H(\sigma)=\frac{\omega(\sigma)}{\overline{\omega'(\sigma)}}=\sum_{n=1}^{m}c_n\sigma^n+h(\sigma), \tag{27}$$

where $h(\sigma)$ is analytic inside the unit circle, and is bounded at the infinite, i.e., $h(\infty)=C$.

Recalling Eq. (5), $\varphi_0(\sigma)$ can be divided into into two parts, i.e.,

$$\varphi_0(\sigma)=\varphi_{0,\mathrm{macro}}(\sigma)+\varphi_{0,\mathrm{micro}}(\sigma).$$

Here, $\varphi_{0,\mathrm{macro}}(\sigma)$ and $\varphi_{0,\mathrm{micro}}(\sigma)$ are both analytic inside the unit circle, and thus could be expressed in polynomial series that $\varphi_{0,\mathrm{macro}}(\sigma)=\sum\limits_{n=1}^{\infty}a_n\sigma^n$ and $\varphi_{0,\mathrm{micro}}(\sigma)=\sum\limits_{n=1}^{\infty}b_n\sigma^n$, respectively. We have

$$\overline{\varphi_0'(\sigma)}=\overline{\varphi_0'}\Big(\frac{1}{\sigma}\Big)=\sum_{n=1}^{\infty}n\overline{a_n}\sigma^{1-n}+\sum_{n=1}^{\infty}n\overline{b_n}\sigma^{1-n}.$$

Together with Eq. (27), the integrand in Eq. (5) could be written as

$$\begin{aligned}\frac{\omega(\sigma)}{\overline{\omega'(\sigma)}}\overline{\varphi_0'(\sigma)}&=\Big(\sum_{j=1}^{m}c_j\sigma^j+h(\sigma)\Big)\Big(\sum_{n=1}^{\infty}n\overline{a_n}\sigma^{1-n}+\sum_{n=1}^{\infty}n\overline{b_n}\sigma^{1-n}\Big)\\&=\sum_{j=1}^{m}\sum_{n=1}^{\infty}n\overline{a_n}c_j\sigma^{1-n+j}+\sum_{j=1}^{m}\sum_{n=1}^{\infty}n\overline{b_n}c_j\sigma^{1-n+j}\\&\quad+\Big(\sum_{n=1}^{\infty}n\overline{a_n}\sigma^{1-n}+\sum_{n=1}^{\infty}n\overline{b_n}\sigma^{1-n}\Big)h(\sigma).\end{aligned} \tag{28}$$

It could further be simplified through Cauchy's integral formula, which yields

$$\begin{aligned}\frac{1}{2\pi\mathrm{i}}\int_\Gamma\frac{\omega(\sigma)}{\overline{\omega'(\sigma)}}\frac{\overline{\varphi_0'(\sigma)}}{\sigma-\zeta}\mathrm{d}\sigma&=\frac{1}{2\pi\mathrm{i}}\int_\Gamma\frac{\sum\limits_{j=1}^{m}\sum\limits_{n=1}^{k}n\overline{a_n}c_j\sigma^{1-n+j}}{\sigma-\zeta}\mathrm{d}\sigma+\frac{1}{2\pi\mathrm{i}}\int_\Gamma\frac{\sum\limits_{j=1}^{m}\sum\limits_{n=1}^{k}n\overline{b_n}c_j\sigma^{1-n+j}}{\sigma-\zeta}\mathrm{d}\sigma\\&\quad+\frac{1}{2\pi\mathrm{i}}\int_\Gamma\frac{\sum\limits_{n=1}^{k}n\overline{a_n}\sigma^{1-n}h(\sigma)}{\sigma-\zeta}\mathrm{d}\sigma+\frac{1}{2\pi\mathrm{i}}\int_\Gamma\frac{\sum\limits_{n=1}^{k}n\overline{a_n}\sigma^{1-n}h(\sigma)}{\sigma-\zeta}\mathrm{d}\sigma\\&=\sum_{j=1}^{m}\sum_{n=1}^{j-1}n\overline{a_n}c_j\zeta^{1-n+j}+\sum_{j=1}^{m}\sum_{n=1}^{j-1}n\overline{b_n}c_j\zeta^{1-n+j}\\&\quad+\frac{1}{2\pi\mathrm{i}}\int_\Gamma\frac{\sum\limits_{n=1}^{k}n\overline{a_n}\sigma^{1-n}h(\sigma)}{\sigma-\zeta}\mathrm{d}\sigma+\frac{1}{2\pi\mathrm{i}}\int_\Gamma\frac{\sum\limits_{n=1}^{k}n\overline{a_n}\sigma^{1-n}h(\sigma)}{\sigma-\zeta}\mathrm{d}\sigma.\end{aligned} \tag{29}$$

Here, we denote $H_1(\sigma)=\sum\limits_{n=1}^{k}n\overline{a_n}\sigma^{1-n}h(\sigma)$ and $H_2(\sigma)=\sum\limits_{n=1}^{k}n\overline{b_n}\sigma^{1-n}h(\sigma)$. It is known that $H_1(\sigma)$ and $H_2(\sigma)$ are analytic in the domain outside the unit circle, including the infinity. Thus, $\sigma=\infty$ is a removable singular point, and

$$\frac{1}{2\pi\mathrm{i}}\int_{\Gamma}\frac{\sum\limits_{n=1}^{k}n\overline{a_n}\sigma^{1-n}h(\sigma)}{\sigma-\zeta}\mathrm{d}\sigma=H_1(\infty)=0,$$
$$\frac{1}{2\pi\mathrm{i}}\int_{\Gamma}\frac{\sum\limits_{n=1}^{k}n\overline{b_n}\sigma^{1-n}h(\sigma)}{\sigma-\zeta}\mathrm{d}\sigma=H_2(\infty)=0.$$

Based on the above results, the first governing equation in Eq. (5) could thus be calculated as

$$\begin{aligned}&\varphi_{0,\mathrm{macro}}(\zeta)+\varphi_{0,\mathrm{micro}}(\zeta)+\sum_{j=1}^{m}\sum_{n=1}^{j-1}n\overline{a_n}c_j\zeta^{1-n+j}+\sum_{j=1}^{m}\sum_{n=1}^{j-1}n\overline{b_n}c_j\zeta^{1-n+j}\\&=\frac{1}{2\pi\mathrm{i}}\int_{\Gamma}\frac{f_{0,\mathrm{macro}}}{\sigma-\zeta}\mathrm{d}\sigma+\frac{1}{2\pi\mathrm{i}}\int_{\Gamma}\frac{f_{0,\mathrm{micro}}}{\sigma-\zeta}\mathrm{d}\sigma.\end{aligned}\tag{30}$$

For a cluster of primary (macro) holes that the highest order in the polynomial expansion of the transformation function $\omega_0(\zeta)$ is no more than 1, named as the simple hole here, $c_j=0$ (m equals zero). The circle ($\omega_0=1/\zeta$) and the ellipse ($\omega_0=1/\zeta+m\zeta$) both fall into this category. The above expression could easily be constituted as

$$\varphi_0=\varphi_{0,\mathrm{macro}}(\zeta)+\varphi_{0,\mathrm{micro}}(\zeta),$$

where

$$\varphi_{0,\mathrm{macro}}(\zeta)=\frac{1}{2\pi\mathrm{i}}\int_{\Gamma}\frac{f_{0,\mathrm{macro}}}{\sigma-\zeta}\mathrm{d}\sigma,\quad\varphi_{0,\mathrm{micro}}(\zeta)=\frac{1}{2\pi\mathrm{i}}\int_{\Gamma}\frac{f_{0,\mathrm{micro}}}{\sigma-\zeta}\mathrm{d}\sigma.\tag{31}$$

For simple-hole cases, the governing equations at macroscopic and microscopic scales could be completely decoupled.

In the general case, the 2nd and 3rd terms in Eq. (30) do not automatically vanish. First, according to Eq. (20), we have

$$\frac{\omega(\sigma)}{\overline{\omega'(\sigma)}}=\frac{\omega_0(\sigma)}{\overline{\omega_0'(\sigma)}}+\frac{\overline{\omega_0'(\sigma)}k\delta(\sigma,\alpha)-\omega_0(\sigma)\overline{k\delta'(\sigma,\alpha)}}{\overline{\omega_0'(\sigma)}\,\overline{\omega'(\sigma)}}\triangleq\frac{\omega_0(\sigma)}{\overline{\omega_0'(\sigma)}}+\Delta_1(\sigma),\tag{32}$$

where $\Delta_1(\sigma)$ is defined as

$$\Delta_1(\sigma)=\frac{\overline{\omega_0'(\sigma)}k\delta(\sigma,\alpha)-\omega_0(\sigma)\overline{k\delta'(\sigma,\alpha)}}{\overline{\omega_0'(\sigma)}\,\overline{\omega'(\sigma)}},\tag{33}$$

and if necessary, $\omega'(\sigma)$ could also be approximately calculated as $\omega_0'(\sigma)+k\delta'(\sigma,\alpha)$.

Substituting it into Eq. (5), it could be achieved that

$$\begin{aligned}&\varphi_{0,\mathrm{macro}}(\sigma)+\varphi_{0,\mathrm{micro}}(\sigma)+\frac{1}{2\pi\mathrm{i}}\int_{\Gamma}\Big(\frac{\omega_0(\sigma)}{\overline{\omega_0'(\sigma)}}+\Delta_1(\sigma)\Big)\Big(\frac{\overline{\varphi_{0,\mathrm{macro}}'(\sigma)}+\overline{\varphi_{0,\mathrm{micro}}'(\sigma)}}{\sigma-\zeta}\Big)\mathrm{d}\sigma\\&=\frac{1}{2\pi\mathrm{i}}\int_{\Gamma}\frac{f_{0,\mathrm{macro}}}{\sigma-\zeta}\mathrm{d}\sigma+\frac{1}{2\pi\mathrm{i}}\int_{\Gamma}\frac{f_{0,\mathrm{micro}}}{\sigma-\zeta}\mathrm{d}\sigma.\end{aligned}\tag{34}$$

By the definition of $\varphi_{0,\mathrm{macro}}(\zeta)$, we have

$$\varphi_{0,\mathrm{macro}}(\zeta)+\frac{1}{2\pi\mathrm{i}}\int_\Gamma \frac{\omega_0(\sigma)}{\overline{\omega_0'(\sigma)}}\frac{\overline{\varphi_{0,\mathrm{macro}}'(\sigma)}}{\sigma-\zeta}\mathrm{d}\sigma=\frac{1}{2\pi\mathrm{i}}\int_\Gamma\frac{f_{0,\mathrm{macro}}}{\sigma-\zeta}\mathrm{d}\sigma, \tag{35}$$

and the governing equation for $\varphi_{0,\mathrm{micro}}(\zeta)$ could thus be extracted,

$$\begin{aligned}&\varphi_{0,\mathrm{micro}}(\zeta)+\frac{1}{2\pi\mathrm{i}}\int_\Gamma\Big(\frac{\omega_0(\sigma)}{\overline{\omega_0'(\sigma)}}+\Delta_1\Big)\frac{\overline{\varphi_{0,\mathrm{micro}}'(\sigma)}}{\sigma-\zeta}\mathrm{d}\sigma\\&=\frac{1}{2\pi\mathrm{i}}\int_\Gamma\frac{(f_{0,\mathrm{micro}}-\Delta_1\overline{\varphi_{0,\mathrm{macro}}'(\sigma)})}{\sigma-\zeta}\mathrm{d}\sigma.\end{aligned} \tag{36}$$

Factors that play roles in determining the potential function at the microscopic scale could be identified from Eq. (36). First, on the left side, the integral kernel has been modified, introducing the deviation of mapping function due to the microscopic edge defect. Also, the macroscopic potential of $\varphi_{0,\mathrm{macro}}$ should be passed into the governing equation at the microscopic level, which could also be treated as a modification to $f_{0,\mathrm{micro}}$. Obviously, when $\omega_{\mathrm{micro}}(\sigma)=0$, i.e., $\delta(\sigma,\alpha)=0$, the complex potential $\varphi_{0,\mathrm{micro}}(\zeta)$ degenerates to zero.

In summary, Eqs. (35) and (36) are the governing equations of the potential φ_0 at the macroscopic and microscopic scales, respectively. $\varphi_{0,\mathrm{macro}}(\zeta)$ is first determined by Eq. (35). Substituting it into Eq. (36), $\varphi_{0,\mathrm{micro}}(\zeta)$ could be calculated. Equation (23) is used to achieve the expression of $\varphi_0(\zeta)$.

In a similar way, the potential function ψ_0 (see Eq. (5)) could also be decoupled,

$$\psi_0(\zeta)=\psi_{0,\mathrm{macro}}(\zeta)+\psi_{0,\mathrm{micro}}(\zeta),$$

where the macro and micro parts are governed, respectively, by

$$\psi_{0,\mathrm{macro}}(\zeta)+\frac{1}{2\pi\mathrm{i}}\int_\Gamma\frac{\overline{\omega_0(\sigma)}}{\overline{\omega_0'(\sigma)}}\frac{\varphi_{0,\mathrm{macro}}'(\sigma)}{\sigma-\zeta}\mathrm{d}\sigma=\frac{1}{2\pi\mathrm{i}}\int_\Gamma\frac{\overline{f_{0,\mathrm{macro}}}}{\sigma-\zeta}\mathrm{d}\sigma \tag{37}$$

and

$$\begin{aligned}&\psi_{0,\mathrm{micro}}(\zeta)+\frac{1}{2\pi\mathrm{i}}\int_\Gamma\Big(\frac{\overline{\omega_0(\sigma)}}{\overline{\omega_0'(\sigma)}}+\overline{\Delta_1}\Big)\frac{\varphi_{0,\mathrm{micro}}'(\sigma)}{\sigma-\zeta}\mathrm{d}\sigma\\&=\frac{1}{2\pi\mathrm{i}}\int_\Gamma\frac{\Big(\overline{f_{0,\mathrm{micro}}}-\overline{\Delta_1}\,\varphi_{0,\mathrm{macro}}'(\sigma)\Big)}{\sigma-\zeta}\mathrm{d}\sigma.\end{aligned} \tag{38}$$

The decoupling of potential functions could be summarized here. First, according to Eq. (22),

$$\varphi(\zeta)=\varphi_{\mathrm{macro}}(\zeta)+\varphi_{\mathrm{micro}}(\zeta),\quad \psi(\zeta)=\psi_{\mathrm{macro}}(\zeta)+\psi_{\mathrm{micro}}(\zeta).$$

Correspondingly, we have

$$\begin{cases}\varphi_{\mathrm{macro}}(\zeta)=B\omega_0(\zeta)+\varphi_{0,\mathrm{macro}}(\zeta),\\ \psi_{\mathrm{macro}}(\zeta)=(B'+\mathrm{i}\,C')\omega_0(\zeta)+\psi_{0,\mathrm{macro}}(\zeta),\end{cases} \tag{39}$$

and

$$\begin{cases}\varphi_{\mathrm{micro}}(\zeta)=B\omega_{\mathrm{micro}}(\zeta)+\varphi_{0,\mathrm{micro}}(\zeta),\\ \psi_{\mathrm{micro}}(\zeta)=(B'+\mathrm{i}\,C')\omega_{\mathrm{micro}}(\zeta)+\psi_{0,\mathrm{micro}}(\zeta),\end{cases} \tag{40}$$

where $\varphi_{0,\mathrm{macro}}$, $\varphi_{0,\mathrm{micro}}$, $\psi_{0,\mathrm{macro}}$, and $\psi_{0,\mathrm{micro}}$ are governed by Eqs. (35)–(38), respectively.

2.4 Determination of stress components

First, we denote the differentiation of $\varphi_1'(z)$ as $\Phi(\zeta)$,

$$\begin{aligned}\Phi(\zeta)=\frac{\varphi'(\zeta)}{\omega'(\zeta)}&=\frac{\varphi'_{\text{macro}}(\zeta)+\varphi'_{\text{micro}}(\zeta)}{\omega'_0(\zeta)+\omega'_{\text{micro}}(\zeta)}=\frac{\varphi'_{\text{macro}}(\zeta)}{\omega'_0(\zeta)}\\&+\frac{\omega'_0(\zeta)\varphi'_{\text{macro}}(\zeta)+\omega'_0(\zeta)\varphi'_{\text{micro}}(\zeta)}{\omega'_0(\zeta)(\omega'_0(\zeta)+\omega'_{\text{micro}}(\zeta))}-\frac{\varphi'_{\text{macro}}(\zeta)\omega'_0(\zeta)+\varphi'_{\text{macro}}(\zeta)\omega'_{\text{micro}}(\zeta)}{\omega'_0(\zeta)(\omega'_0(\zeta)+\omega'_{\text{micro}}(\zeta))}\\&=\frac{\varphi'_{\text{macro}}(\zeta)}{\omega'_0(\zeta)}+\frac{\omega'_0(\zeta)\varphi'_{\text{micro}}(\zeta)-\varphi'_{\text{macro}}(\zeta)\omega'_{\text{micro}}(\zeta)}{\omega'_0(\zeta)(\omega'_0(\zeta)+\omega'_{\text{micro}}(\zeta))}.\end{aligned}$$

It could be separated in the form of

$$\Phi(\zeta)=\Phi_{\text{macro}}(\zeta)+\Phi_{\text{micro}}(\zeta),\tag{41}$$

where

$$\begin{cases}\Phi_{\text{macro}}(\zeta)=\dfrac{\varphi'_{\text{macro}}(\zeta)}{\omega'_0(\zeta)},\\[2ex]\Phi_{\text{micro}}(\zeta)=\dfrac{\omega'_0(\zeta)\varphi'_{\text{micro}}(\zeta)-\varphi'_{\text{macro}}(\zeta)\omega'_{\text{micro}}(\zeta)}{\omega'_0(\zeta)(\omega'_0(\zeta)+\omega'_{\text{micro}}(\zeta))}.\end{cases}\tag{42}$$

Similarly, the differentiation of $\psi_1(z)$ could also be separated

$$\Psi(\zeta)=\frac{\psi'(\zeta)}{\omega'(\zeta)}=\Psi_{\text{macro}}(\zeta)+\Psi_{\text{micro}}(\zeta),\tag{43}$$

where

$$\begin{cases}\Psi_{\text{macro}}(\zeta)=\dfrac{\psi'_{\text{macro}}(\zeta)}{\omega'_0(\zeta)},\\[2ex]\Psi_{\text{micro}}(\zeta)=\dfrac{\omega'_0(\zeta)\psi'_{\text{micro}}(\zeta)-\psi'_{\text{macro}}(\zeta)\omega'_{\text{micro}}(\zeta)}{\omega'_0(\zeta)(\omega'_0(\zeta)+\omega'_{\text{micro}}(\zeta))}.\end{cases}\tag{44}$$

The stress could thus be calculated as follows:

$$\sigma_\theta+\sigma_\rho=4\text{Re}\frac{\varphi'(\zeta)}{\omega'(\zeta)}=4\text{Re}\Phi_{\text{macro}}(\zeta)+4\text{Re}\Phi_{\text{micro}}(\zeta),\tag{45}$$

and

$$\begin{aligned}\sigma_\theta-\sigma_\rho+2\text{i}\tau_{\rho\theta}&=\frac{2\zeta}{\overline{\zeta\omega'(\zeta)}}(\overline{\omega(\zeta)}\Phi'(\zeta)+\omega'(\zeta)\Psi(\zeta))\\&=\frac{2\zeta}{\overline{\zeta}(\overline{\omega'_0(\zeta)}+\overline{\omega'_{\text{micro}}(\zeta)})}((\overline{\omega_0(\zeta)}+\overline{\omega_{\text{micro}}(\zeta)})(\Phi'_{\text{macro}}(\zeta)+\Phi'_{\text{micro}}(\zeta))\\&\quad+(\omega'_0(\zeta)+\omega'_{\text{micro}}(\zeta))(\Psi_{\text{macro}}(\zeta)+\Psi_{\text{micro}}(\zeta))).\end{aligned}\tag{46}$$

It could be expanded as

$$\begin{aligned}\sigma_\theta-\sigma_\rho+2\text{i}\tau_{\rho\theta}&=\frac{2\zeta}{\overline{\zeta\omega'(\zeta)}}(\overline{\omega(\zeta)}\Phi'(\zeta)+\omega'(\zeta)\Psi(\zeta))\\&=\frac{2\zeta}{\overline{\zeta}(\overline{\omega'_0(\zeta)}+\overline{\omega'_{\text{micro}}(\zeta)})}((\overline{\omega_0(\zeta)}+\overline{\omega_{\text{micro}}(\zeta)})(\Phi'_{\text{macro}}(\zeta)+\Phi'_{\text{micro}}(\zeta))\\&\quad+(\omega'_0(\zeta)+\omega'_{\text{micro}}(\zeta))(\Psi_{\text{macro}}(\zeta)+\Psi_{\text{micro}}(\zeta)))\\&=\frac{2\zeta}{\overline{\zeta}}\Big(\frac{1}{\overline{\omega'_0(\zeta)}}-\frac{\overline{\omega'_{\text{micro}}(\zeta)}}{\overline{\omega'_0(\zeta)}(\overline{\omega'_0(\zeta)}+\overline{\omega'_{\text{micro}}(\zeta)})}\Big)\Big(\overline{\omega_0(\zeta)}\Phi'_{\text{macro}}(\zeta)+\overline{\omega_0(\zeta)}\Phi'_{\text{micro}}(\zeta)\\&\quad+\overline{\omega_{\text{micro}}(\zeta)}\Phi'_{\text{macro}}(\zeta)+\overline{\omega_{\text{micro}}(\zeta)}\Phi'_{\text{micro}}(\zeta)+\omega'_0(\zeta)\Psi_{\text{macro}}(\zeta)\\&\quad+\omega'_0(\zeta)\Psi_{\text{micro}}(\zeta)+\omega'_{\text{micro}}(\zeta)\Psi_{\text{macro}}(\zeta)+\omega'_{\text{micro}}(\zeta)\Psi_{\text{micro}}(\zeta)\Big).\end{aligned}$$

In order to simplify the above formula, we define

$$\begin{aligned}\Delta_3 =&\overline{\omega_0(\zeta)}\Phi'_{\rm micro}(\zeta)+\overline{\omega_{\rm micro}(\zeta)}\Phi'_{\rm macro}(\zeta)+\overline{\omega_{\rm micro}(\zeta)}\Phi'_{\rm micro}(\zeta)\\&+\omega'_0(\zeta)\Psi_{\rm micro}(\zeta)+\omega'_{\rm micro}(\zeta)\Psi_{\rm macro}(\zeta)+\omega'_{\rm micro}(\zeta)\Psi_{\rm micro}(\zeta).\end{aligned}\tag{47}$$

The above equation could be written as

$$\begin{aligned}&\sigma_\theta-\sigma_\rho+2{\rm i}\tau_{\rho\theta}\\=&\frac{2\zeta}{\overline{\zeta\omega'(\zeta)}}(\overline{\omega(\zeta)}\Phi'(\zeta)+\omega'(\zeta)\Psi(\zeta))\\=&\frac{2\zeta}{\overline{\zeta}}\Big(\frac{1}{\overline{\omega'_0(\zeta)}}-\frac{\overline{\omega'_{\rm micro}(\zeta)}}{\overline{\omega'_0(\zeta)}(\overline{\omega'_0(\zeta)}+\overline{\omega'_{\rm micro}(\zeta)})}\Big)\Big(\overline{\omega_0(\zeta)}\Phi'_{\rm macro}(\zeta)+\omega'_0(\zeta)\Psi_{\rm macro}(\zeta)+\Delta_3\Big)\\=&\frac{2\zeta}{\overline{\zeta\omega'_0(\zeta)}}(\overline{\omega_0(\zeta)}\Phi'_{\rm macro}(\zeta)+\omega'_0(\zeta)\Psi_{\rm macro}(\zeta))+\frac{2\zeta}{\overline{\zeta\omega'_0(\zeta)}}\Delta_3\\&-\frac{2\zeta}{\overline{\zeta}}\frac{\overline{\omega'_{\rm micro}(\zeta)}}{\overline{\omega'_0(\zeta)}(\overline{\omega'_0(\zeta)}+\overline{\omega'_{\rm micro}(\zeta)})}\Big(\overline{\omega_0(\zeta)}\Phi'_{\rm macro}(\zeta)+\omega'_0(\zeta)\Psi_{\rm macro}(\zeta)+\Delta_3\Big).\end{aligned}\tag{48}$$

Equations (45) and (48) could be split into two parts, namely,

$$\sigma_{ij}=\sigma_{ij}^{\rm macro}+\sigma_{ij}^{\rm micro},\quad i,j=\rho,\theta,\tag{49}$$

where the macro part is naturally defined as

$$\begin{cases}\sigma_\theta^{\rm macro}+\sigma_\rho^{\rm macro}=4{\rm Re}\dfrac{\varphi'_0(\zeta)}{\omega'_0(\zeta)}=4{\rm Re}\Phi_{\rm macro}(\zeta),\\ \sigma_\theta^{\rm macro}-\sigma_\rho^{\rm macro}+2{\rm i}\tau_{\rho\theta}^{\rm macro}=\dfrac{2\zeta}{\overline{\zeta\omega'_0(\zeta)}}(\overline{\omega_0(\zeta)}\Phi'_{\rm macro}(\zeta)+\omega'_0(\zeta)\Psi_{\rm macro}(\zeta)).\end{cases}\tag{50}$$

Substituting the above equation into Eqs. (45) and (48), the micro level of stress expressions could be extracted,

$$\sigma_\theta^{\rm micro}+\sigma_\rho^{\rm micro}=4{\rm Re}\Phi_{\rm micro}(\zeta),\tag{51}$$

$$\begin{aligned}&\sigma_\theta^{\rm micro}-\sigma_\rho^{\rm micro}+2{\rm i}\tau_{\rho\theta}^{\rm micro}\\=&\frac{2\zeta}{\overline{\zeta\omega'_0(\zeta)}}\Big(\frac{\overline{\omega'_0(\zeta)}}{(\overline{\omega'_0(\zeta)}+\overline{\omega'_{\rm micro}(\zeta)})}\Delta_3\\&-\frac{\overline{\omega'_{\rm micro}(\zeta)}}{(\overline{\omega'_0(\zeta)}+\overline{\omega'_{\rm micro}(\zeta)})}\Big(\overline{\omega_0(\zeta)}\Phi'_{\rm macro}(\zeta)+\omega'_0(\zeta)\Psi_{\rm macro}(\zeta)\Big)\Big).\end{aligned}\tag{52}$$

Combining Eqs. (50) and (51), the stress field is distinctively solved, where the micro part could be seen as a deviation (or perturbation) from the macro part due to the existence of microscopic edge effect, making it possible to evaluate its effect on global behaviors. Also, the macro part of stress would turn zero when $\omega_{\rm micro}(\zeta)=0$, which coincides with the actual situation.

3 Multiscale framework application: an elliptic hole with single edge defect

In engineering practice, inclusions or certain defects can be simplified as elliptic holes. The problem stated here is an elliptic hole (the primary defect) with an semicircular edge defect (the secondary defect). The adjacent primary and secondary defects are thus referred to as hierarchical defects. It should be noted that the framework is applicable for any other shapes of primary and secondary defects.

3.1 Mapping functions for semicircular micro-defect

First, an infinite plate containing a circular hole (unit size) and a semicircular edge defect (radius of $\rho \ll 1$) at $z = 1$ is considered, as shown in Fig. 1(a) or Fig. A1. The transformation that maps the above domain Ω (the z-plane) into a unit disk D (the ζ-plane) is written below. The details could be found in Appendix A.

$$z = \omega(\zeta) = \frac{\zeta + 1}{2\zeta} + \frac{\sqrt{(\zeta - 1)^2 + 4\rho^2\zeta}}{2\zeta}, \tag{53}$$

where $\omega(\zeta)$ is a multi-valued function, and the branch of $\sqrt{-1} = \mathrm{i}$ is chosen here. It could be verified that when $\rho = 0$, the above equation will be degenerated to $1/\zeta$, which is exactly the mapping function for the classical solution of circular hole.

The deviation of mapping function could thus be obtained through Eq. (13),

$$\delta(\zeta) = \omega(\zeta) - \frac{1}{\zeta} = \frac{\zeta - 1}{2\zeta} + \frac{\sqrt{(\zeta - 1)^2 + 4\rho^2\zeta}}{2\zeta}. \tag{54}$$

The micro-defect location could also be taken into account by Eq. (14), allowing $\delta(\zeta)$ to be generalized as

$$\delta(\zeta, \alpha) = \mathrm{e}^{\mathrm{i}\alpha}\omega(\mathrm{e}^{\mathrm{i}\alpha}\zeta) - \frac{1}{\zeta} = \frac{\mathrm{e}^{\mathrm{i}\alpha}\zeta - 1}{2\zeta} + \frac{\sqrt{(\mathrm{e}^{\mathrm{i}\alpha}\zeta - 1)^2 + 4\rho^2\mathrm{e}^{\mathrm{i}\alpha}\zeta}}{2\zeta}. \tag{55}$$

$\delta(\zeta, \alpha)$ has two branch points on the unit circle around the location of $\mathrm{e}^{-\mathrm{i}\alpha}$, denoted as ζ_1 and ζ_1, respectively.

$$\zeta_{1,2} = \mathrm{e}^{-\mathrm{i}\alpha}(1 - 2\rho^2 \pm 2\sqrt{\rho^4 - \rho^2}). \tag{56}$$

As seen in Fig. 1(c), the short arc linking the two branch points (the ζ-plane) is mapped to the semicircular arc in the z-plane.

This ideal problem could be directly solved using the formulae presented in Subsection 2.1, without using the multiscale framework presented in this article. Here, we briefly give the solution for comparison. It is assumed that the plate is subject to a uniformly remote force of q parallel to the y-axis, which allows Eqs. (8) and (9) to be

$$\varphi(\zeta) = \frac{q}{4}\omega(\zeta) + \varphi_0(\zeta), \quad \psi(\zeta) = \frac{q}{2}\omega(\zeta) + \psi_0(\zeta), \quad f_0 = -\frac{q}{2}\omega(\zeta) - \frac{q}{2}\overline{\omega(\zeta)}. \tag{57}$$

$H(\sigma)$ of Eq. (27) could be calculated as

$$H(\sigma) = \frac{\omega(\sigma)}{\overline{\omega'(\sigma)}} = \frac{\sqrt{\frac{(-1+\sigma)^2+4\rho^2\sigma}{\sigma^2}}(1 + \sigma + (-1+\sigma)^2 + 4\rho^2\sigma)}{\sigma^2\Big(2\rho^2 + \Big(-1 + \sigma + \sigma\sqrt{1 + \frac{1}{\sigma^2} + \frac{-2+4\rho^2}{\sigma}}\Big)\Big)}. \tag{58}$$

It could be verified that the integral on the left-side of Eq. (5) equals zero,

$$\frac{1}{2\pi\mathrm{i}}\int_\Gamma \frac{\omega(\sigma)}{\overline{\omega'(\sigma)}}\frac{\overline{\varphi_0'(\sigma)}}{\sigma - \zeta}\mathrm{d}\sigma = 0, \tag{59}$$

which suggests that

$$\varphi_0(\zeta) = \frac{1}{2\pi\mathrm{i}}\int_\Gamma \frac{f_0}{\sigma - \zeta}\mathrm{d}\sigma = -\frac{q}{2}\frac{1}{2\pi\mathrm{i}}\int_\Gamma \frac{\omega(\sigma) + \overline{\omega(\sigma)}}{\sigma - \zeta}\mathrm{d}\sigma. \tag{60}$$

$\omega(\zeta)$ is analytic in the punctured unit disk $D \setminus \{0\}$, and has a simple pole at 0. Therefore, it could be expanded by the Laurent series in the disk,

$$\omega(\zeta) = \frac{1}{\zeta} + \sum_{n=0}^{\infty} b_n \zeta^n, \tag{61}$$

where b_n are complex constants. According to the Cauchy integral formula, Eq. (5) is reduced to

$$\varphi_0(\zeta) = \frac{1}{2\pi \mathrm{i}} \int_{\Gamma} \frac{f_0}{\sigma - \zeta} \mathrm{d}\sigma = -\frac{q}{2}\Big(\zeta + \omega(\zeta) - \frac{1}{\zeta}\Big), \tag{62}$$

and

$$\psi_0(\zeta) = -\frac{\omega(1/\zeta\,)}{\omega'(\zeta)} \varphi_0'(\zeta) - \frac{q}{2}\Big(\zeta + \omega(\zeta) - \frac{1}{\zeta}\Big). \tag{63}$$

Through further computation from Eq. (11), the SCF for this problem could be achieved,

$$K = \frac{\sigma_{\max}}{q} = \frac{7 - \rho}{1 + \rho}. \tag{64}$$

3.2 Solutions of complex potentials and stresses

First, it has been known that the transformation for mapping an ideally elliptic-holed infinite plane into a unit disk is

$$z_0 = \omega_0(\zeta) = R\Big(\frac{1}{\zeta} + m\zeta\Big). \tag{65}$$

Here, $R = \frac{a+b}{2}$, and $m = \frac{a-b}{a+b}$, where $2a$ and $2b$ are the width and the height of the ellipse, respectively.

Following Eq. (17) or (18), the overall mapping function could be constructed as follows:

$$\omega(\zeta) = \omega_0\big(\omega^*(\zeta)\big) = \omega_0(\zeta) + R(1 - m\zeta^2)\delta(\zeta, \alpha), \tag{66}$$

where $\delta(\zeta, \alpha)$ could be found in Eq. (55). Due to the compactly supported property of δ function (at $\zeta = \mathrm{e}^{-\mathrm{i}\alpha}$), the above transformation could also be approximately written as

$$z = \omega(\zeta) = \omega_0(\zeta) + k\delta(\zeta, \alpha), \tag{67}$$

where $k = R(1 - m\mathrm{e}^{-2\mathrm{i}\alpha})$ is the scaling factor. It is found that the actual radius of the micro-defect is

$$r \approx |k|\, \rho. \tag{68}$$

Figure 3 shows an example of the transformation. The branch points located in the neighborhood of $\zeta = \mathrm{e}^{-\mathrm{i}\alpha}$ are $\zeta_{1,2} = \mathrm{e}^{-\mathrm{i}\alpha}(1 - 2\rho^2 \pm 2\sqrt{\rho^4 - \rho^2})$, which are mapped to the two points where the microscale circle intersects with the ellipse, i.e., Points B and C.

To exactly locate the micro-defect, the relationship of the radial angles between the two coordinate systems is provided,

$$\beta = \mathrm{Arg}((a + b)\mathrm{e}^{\mathrm{i}\alpha} + (a - b)\mathrm{e}^{-\mathrm{i}\alpha}), \tag{69}$$

where β is the angle between the x-axis and the center of the micro-defect (the z-plane).

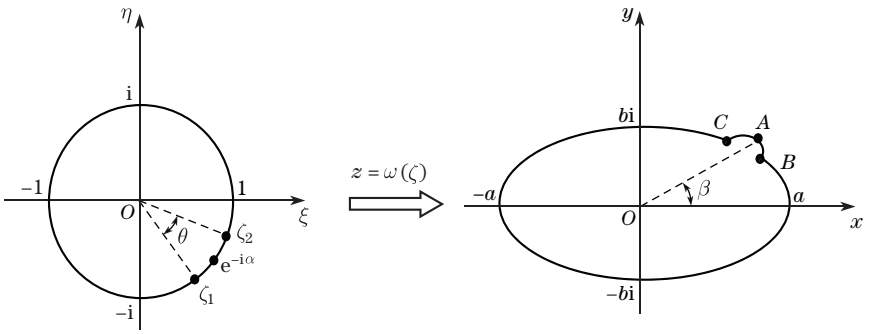

Fig. 3 Polar angles in the ζ-plane and the z-plane

Based on the above preparations, the potentials and stresses are ready to be solved. Since the elliptic hole is a simple hole, Eq. (31) is adopted.

$$\begin{cases} \varphi_{0,\mathrm{macro}}(\zeta) = \dfrac{1}{2\pi\mathrm{i}}\displaystyle\int_\Gamma \frac{f_{0,\mathrm{macro}}}{\sigma-\zeta}\mathrm{d}\sigma = -\frac{q}{2}\frac{1}{2\pi\mathrm{i}}\int_\Gamma \frac{\omega_0(\sigma)-\overline{\omega_0(\sigma)}\mathrm{e}^{2\mathrm{i}\gamma}}{\sigma-\zeta}\mathrm{d}\sigma, \\ \varphi_{0,\mathrm{micro}}(\zeta) = \dfrac{1}{2\pi\mathrm{i}}\displaystyle\int_\Gamma \frac{f_{0,\mathrm{micro}}}{\sigma-\zeta}\mathrm{d}\sigma = -\frac{q}{2}\frac{1}{2\pi\mathrm{i}}\int_\Gamma \frac{k\delta(\sigma,\alpha)-\overline{k\delta(\sigma,\alpha)}\mathrm{e}^{2\mathrm{i}\gamma}}{\sigma-\zeta}\mathrm{d}\sigma. \end{cases} \tag{70}$$

Here, $\delta(\zeta,\alpha)$ is analytic in the punctured unit disk, and $\zeta=0$ is a removable pole. Hence, it could be expressed in the form of Taylor series within the open unit disk,

$$\delta(\zeta,\alpha) = \sum_{n=0}^{\infty} c_n(\alpha)\zeta^n, \tag{71}$$

where c_n are complex constants related to α.

Using the Cauchy integral formula, we have

$$\frac{1}{2\pi\mathrm{i}}\int_\Gamma \frac{\delta(\sigma,\alpha)}{\sigma-\zeta}\mathrm{d}\sigma = \delta(\zeta,\alpha), \quad \frac{1}{2\pi\mathrm{i}}\int_\Gamma \frac{\overline{\delta(\sigma,\alpha)}}{\sigma-\zeta}\mathrm{d}\sigma = 0. \tag{72}$$

Then, Eq. (70) is

$$\begin{cases} \varphi_{0,\mathrm{macro}}(\zeta) = \dfrac{1}{2\pi\mathrm{i}}\displaystyle\int_\Gamma \frac{f_{0,\mathrm{macro}}}{\sigma-\zeta}\mathrm{d}\sigma = -\frac{q}{2}R(m-\mathrm{e}^{2\mathrm{i}\gamma})\zeta, \\ \varphi_{0,\mathrm{micro}}(\zeta) = \dfrac{1}{2\pi\mathrm{i}}\displaystyle\int_\Gamma \frac{f_{0,\mathrm{micro}}}{\sigma-\zeta}\mathrm{d}\sigma = -\frac{q}{2}k\delta(\zeta,\alpha). \end{cases} \tag{73}$$

Through similar integral operations, $\psi_0(\zeta)$ could be obtained as follows:

$$\begin{aligned} \psi_{0,\mathrm{macro}}(\zeta) &= -\frac{qR}{2}((1-m\mathrm{e}^{-2\mathrm{i}\gamma})\zeta) - \frac{\omega_0(1/\zeta)}{\omega_0'(\zeta)}\varphi_{0,\mathrm{macro}}'(\zeta) \\ &= -\frac{qR}{2}\Big((1-m\mathrm{e}^{-2\mathrm{i}\gamma})\zeta + (m-\mathrm{e}^{2\mathrm{i}\gamma})\frac{m+\zeta^2}{1-m\zeta^2}\zeta\Big), \end{aligned} \tag{74}$$

$$\begin{aligned} \psi_{0,\mathrm{micro}}(\zeta) &= \frac{q}{2}k\delta(\zeta,\alpha)\mathrm{e}^{-2\mathrm{i}\gamma} - \frac{\omega_0(1/\zeta)+\overline{k}\delta(1/\zeta,-\alpha)}{\omega_0'(\zeta)+k\delta'(\zeta,\alpha)}\varphi_{0,\mathrm{micro}}'(\zeta) \\ &\quad + \frac{\omega_0(1/\zeta)k\delta'(\zeta,\alpha)-\omega_0'(\zeta)\overline{k}\delta(1/\zeta,-\alpha)}{\omega_0'(\zeta)(\omega_0'(\zeta)+k\delta'(\zeta,\alpha))}\varphi_{0,\mathrm{macro}}'(\zeta). \end{aligned} \tag{75}$$

The macroscale part of the stress components in the curvilinear coordinates could be calculated through Eq. (50) as follows:

$$\begin{aligned}
&\sigma_\theta^{\text{macro}}+\sigma_\rho^{\text{macro}}=q\,\text{Re}\,\frac{(2\text{e}^{2\text{i}\gamma}-m)\zeta^2-1}{m\zeta^2-1},\\
&\sigma_\theta^{\text{macro}}-\sigma_\rho^{\text{macro}}+2\text{i}\tau_{\rho\theta}=q\frac{(m\rho_1^4+\zeta^2)\zeta^2}{\rho_1^4(m-\zeta^2/\rho_1^4\,)(m\zeta^2-1)}\Big(2\text{e}^{2\text{i}\gamma}-m+m\frac{1+m\zeta^2-2\text{e}^{2\text{i}\gamma}\zeta^2}{m\zeta^2-1}\Big)\\
&\qquad\qquad+\frac{q}{\rho_1^2(m-\zeta^2/\rho_1^4\,)}\Big(\text{e}^{-2\text{i}\gamma}-\frac{3\text{e}^{2\text{i}\gamma}\zeta^2+m\text{e}^{2\text{i}\gamma}-m^2-1}{m\zeta^2-1}\zeta^2\\
&\qquad\qquad+\frac{\text{e}^{2\text{i}\gamma}\zeta^2+m\text{e}^{2\text{i}\gamma}-m^2-1}{(m\zeta^2-1)^2}2m\zeta^4\Big),
\end{aligned}\tag{76}$$

where $\rho_1=|\zeta|$ is the radial coordinate in the ζ-plane. Equation (76) is exactly the same as the classical solutions. The microscale part of the stress which is seen as a deviation from the macroscopic part could be calculated from Eq. (51),

$$\begin{aligned}
&\sigma_\theta^{\text{micro}}+\sigma_\rho^{\text{micro}}\\
&=4\,\text{Re}\,\Phi_{\text{micro}}(\zeta)\\
&=4\,\text{Re}\,\Big(\frac{\omega_0'(\zeta)\varphi'_{\text{micro}}(\zeta)-k\delta'(\zeta,\alpha)\varphi'_{\text{macro}}(\zeta)}{\omega_0'(\zeta)(\omega_0'(\zeta)+k\delta'(\zeta,\alpha))}\Big).
\end{aligned}\tag{77}$$

Substituting the expressions of $\varphi'_{\text{macro}}(\zeta)$ and $\varphi'_{\text{micro}}(\zeta)$ into the above equation, we have

$$\begin{aligned}
\sigma_\theta^{\text{micro}}+\sigma_\rho^{\text{micro}}&=4\,\text{Re}\,\Big(\frac{\omega_0'(\zeta)\varphi'_{\text{micro}}(\zeta)-k\delta'(\zeta,\alpha)\varphi'_{\text{macro}}(\zeta)}{\omega_0'(\zeta)(\omega_0'(\zeta)+k\delta'(\zeta,\alpha))}\Big)\\
&=q\,\text{Re}\,\Big(\frac{-k\delta(\zeta,\alpha)\omega_0'(\zeta)-k\delta'(\zeta,\alpha)(\omega_0'(\zeta)-2R(m-\text{e}^{2\text{i}\alpha_1})\zeta)}{\omega_0'(\zeta)(\omega_0'(\zeta)+k\delta'(\zeta,\alpha))}\Big).
\end{aligned}\tag{78}$$

According to Eq. (47),

$$\begin{aligned}
\Delta_3=&\overline{\omega_0(\zeta)}\Phi'_{\text{micro}}(\zeta)+\overline{k\delta(\zeta,\alpha)}\Phi'_{\text{macro}}(\zeta)+\overline{k\delta(\zeta,\alpha)}\Phi'_{\text{micro}}(\zeta)\\
&+\omega_0'(\zeta)\Psi_{\text{micro}}(\zeta)+k\delta'(\zeta,\alpha)\Psi_{\text{macro}}(\zeta)+k\delta'(\zeta,\alpha)\Psi_{\text{micro}}(\zeta),
\end{aligned}$$

the micro part of the stress field in Eq. (52) could be calculated as follows:

$$\begin{aligned}
\sigma_\theta^{\text{micro}}-\sigma_\rho^{\text{micro}}+2\text{i}\tau_{\rho\theta}^{\text{micro}}=&\frac{2\zeta}{\overline{\zeta}(\overline{\omega_0'(\zeta)}+\overline{\omega'_{\text{micro}}(\zeta)})}\Delta_3-\frac{2\zeta\overline{\omega'_{\text{micro}}(\zeta)}}{\overline{\zeta\omega_0'(\zeta)}(\overline{\omega_0'(\zeta)}+\overline{\omega'_{\text{micro}}(\zeta)})}\\
&\cdot(\overline{\omega_0(\zeta)}\Phi'_{\text{macro}}(\zeta)+\omega_0'(\zeta)\Psi_{\text{macro}}(\zeta)).
\end{aligned}\tag{79}$$

3.3 Results and discussion

As an example, Fig. 4 shows the contours of the micro part of the circumferential stress $\sigma_\theta^{\text{micro}}$ and the global part with the parameters of $a=3\,\text{mm}$, $b=1\,\text{mm}$, $\alpha=0$, $\gamma=\pi/2$, $\rho=0.1$, and $q=1\,\text{MPa}$. It is graphically displayed that the micro part of the stress field $\sigma_\theta^{\text{micro}}$ is appreciable around the micro-defect, while in the area afar, the stress can be ignored, indicating that the influence of micro-defect is more local but not negligible. It is noteworthy that $\sigma_\theta^{\text{micro}}$ at the corner between the elliptic hole and circular micro-defect is negative, which guarantees the corner stress be zero in overall (the macro part of stress at the corner is obviously positive).

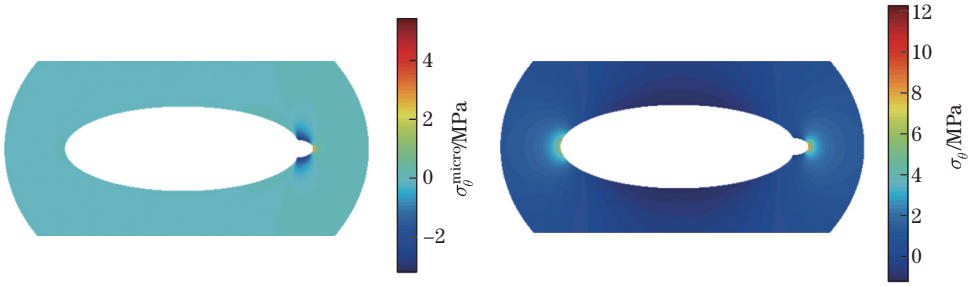

(a) Microscale part $\sigma_\theta^{\text{micro}}$ (b) Overall σ_θ

Fig. 4 Stress contours (color online)

The level of stress concentration around the primary hole is significantly affected by the presence of micro-defect. Here, we focus on investigating the situation of micro-defect located at the long axis (the x-axis) of the elliptic hole, i.e., $\alpha = 0$. Here, $a = 3\,\text{mm}$, $b = 1\,\text{mm}$, and the actual size of micro-defect is equal to the parameter of ρ (in the ζ-plane),

$$r \approx |k|\,\rho = b\rho = \rho.$$

Figure 5 shows the stress concentrations in front of the micro-defect with the changes of the remote tensile direction γ and the defect radius ρ. To investigate the influence of micro effect, an additional SCF caused by the microscale stress field is especially extracted and plotted in Fig. 5 with dashed lines.

$$K_{\text{micro}} = \sigma_{\theta,\text{front}}^{\text{micro}}/q. \tag{80}$$

Besides that, the original value of the SCF without considering the micro-defect is denoted as K_0. It actually equals K_{macro}, if it is defined in a similar way that $K_{\text{macro}} = \sigma_{\theta,\text{front}}^{\text{macro}}/q$. K_0, as plotted with solid lines in Fig. 5, proves the independence of the micro-defect existence. The overall SCF is the summation of K_0 and K_{micro},

$$K = K_0 + K_{\text{micro}}. \tag{81}$$

Here, the curve of K_0 (the SCF in the case of no micro-defect) coincides with the classic solution for elliptic holes[27]. Furthermore, it could be seen that the smaller the micro-defect, the larger stress concentration it contributes. When $\rho = 0.01$, K_{micro} contributed by the micro-defect overtakes the original K_0. Also, the stress at the front of the defect increases with the angle γ of the remote force, reaching its maximum when the remote stress is parallel to the y-axis, or perpendicular to the long axis. In the condition of γ parallel to the long axis, K_{micro} is shown to be zero, indicating that the defect has no extra contribution to the original stress concentration.

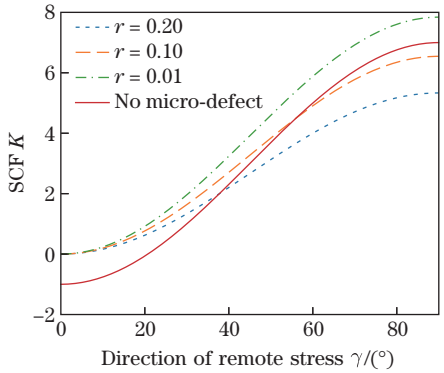

Fig. 5 Influence of micro-defect on the SCF (color online)

Here, the attention is paid to a special condition of $\gamma = 90°$ for it has the greatest SCF among all directions of remote forces. Through further calculation, the relationship between the defect size r and the overall SCF K could be obtained as follows:

$$K = \frac{4a + 3b - r}{b + r}. \tag{82}$$

In the special case of $a = b = 1$, it agrees well with Eq. (64). When r is sufficiently small, the SCF approaches $3 + 4a/b$. In comparison to $K_0 = 1 + 2a/b$ (Inglis's solution[28]), we suggest a modified formula to estimate the stress concentrations when it comes to evaluate the possible effect of microscopic edge defect on the safety of holed structures

$$K_{\mathrm{u}} = 1 + 2K_0. \tag{83}$$

As shown in Fig. 6, the effect of micro-defect location on the SCF is also investigated. K_{micro} reaches its maximum when micro-defect occurs on the long axis, i.e., $\beta = 0°$. It decreases with the increase in β, gradually falls to zero when $\beta = 90°$. It shall also be noted that the maximum influence on the SCF does not exceed 8, even the micro-defect might be very small, which could be validated from Eq. (82).

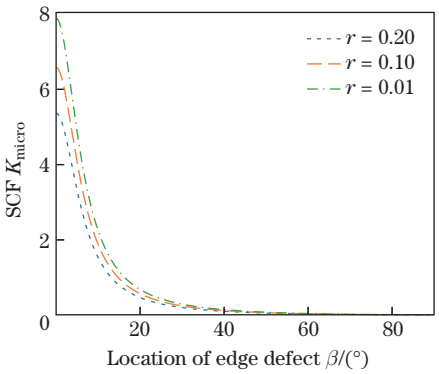

Fig. 6 Location of edge defect and the increase in the SCF (color online)

The affecting area of micro-defect on the stress field is also investigated. Figure 7 provides the change of the normalized circumferential stress $\sigma_\theta^{\mathrm{micro}}/q$ along with the radial distance to the micro-defect front. It clearly shows that the stress decreases rapidly with the increase in the distance, suggesting that the influence along the radial direction is fairly local. Also, Fig. 8 shows the normalized circumferential stress on the hole edge, where the micro-defect is located at $\alpha = 45°$ (i.e., $\beta = 18.4°$) and $\rho = 0.1$. It is graphically displayed that in the circumferential direction (described by its polar angle β in the z-plane), the influence area is mainly between $0°$ and $50°$.

The scale effect cannot be overemphasized in the proposed multiscale framework. At this stage, we mainly focus on solving the designated problems with the features of hierarchical defects. It is stipulated that the size of secondary defect is far smaller than the primary defect. We investigate the relative defect sizes varying from 0.01 to 0.2. It could be verified that under these situations, the separated form of conforming mapping, as shown from Eqs. (16)–(18), agrees well with the exact defect boundary. Since the conformal mapping is the key procedure in solving holed problems, using the complex variable method, the exact stress field could be guaranteed through the exact mapping function.

It is undeniable that quantitatively studying the size range of micro-defect within the multiscale framework is rather challenging. First of all, if the lower bound of the micro-defect

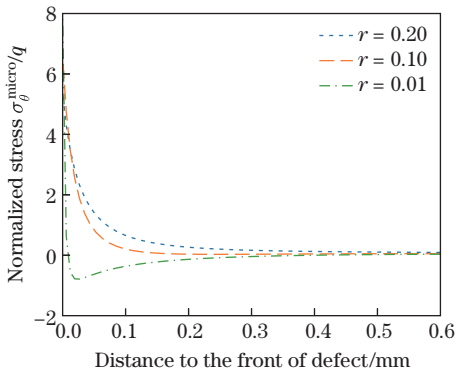

Fig. 7 Variation of the normalized stress with the change of the radial location (color online)

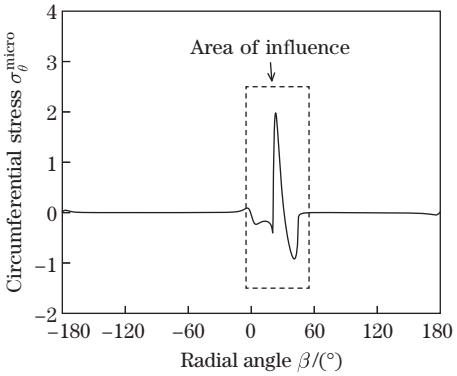

Fig. 8 Variation of the normalized stress with the change of the circumferential location

size is unlimited, according to the formulation between Eqs. (17) and (18), a smaller size of micro-defect naturally leads to a more accurate approximation (see Eq. (18)), while for the upper bound of micro-defect size, several factors may influence the accuracy of the approximation, including the shape of the macro-hole that is expressed in the mapping function of Eq. (16), the relative size of micro-defect expressed in the asymptotical expansion next to Eq. (17), and the local curvature of the macro-defect boundary at the micro-defect location (as expressed in Eq. (8)). Quantitatively defining an upper bound of the micro-defect size is not within the scope of the present framework, which will be left for our forthcoming work.

It is also noted that for the micro-defect size, approaching zero and being zero are two different cases in terms of the stress distribution. The presence of micro-defects causes the stress concentration, regardless of the micro-defect size. When r is sufficiently small, the overall SCF approaches $3+4a/b$, as shown in Eq. (82). If r is directly set to be zero, Eqs. (18) and (53) (the conformal mapping), as well as Eqs. (51) and (52) (the stress solution), are automatically degenerated to the case of no edge defect, meaning that no extra stress concentration occurs.

A similar situation is the classical problem of stress concentration of a holed continuum. Taking the axial tension for example, if a circular hole is small enough, the SCF is constantly $K = 3$, even its size will approach zero. However, in the limit state of no hole, there is obviously no stress concentration at all.

4 Multiscale framework application: a problem with multiple edge defects

One of the advantages of the multiscale framework is to treat the hierarchical problem with multiple edge defects. Under this situation, the mapping function is hard to be exactly constructed via ordinary methods. However, starting from the proposed multiscale framework, micro-defects could be superimposed, which simplifies the process of finding the mapping function and the forthcoming solutions of the stress field.

4.1 Conformal mapping and governing equations

Assuming that there are n different defects existing on the edge of the primary defect, denoted as $\zeta = \mathrm{e}^{\mathrm{i}\alpha_n}$ $(n = 1, 2, \cdots)$, the transformation for multiple edge defects could be constructed by extending Eq. (17) to a general form,

$$z = \omega(\zeta) = \omega_0\Big(\frac{1}{1/\zeta + \delta_1(\zeta, \alpha_1) + \delta_2(\zeta, \alpha_2) + \cdots + \delta_n(\zeta, \alpha_n)}\Big). \tag{84}$$

Ignoring the terms higher than the order of 2, the above function is expanded as

$$\begin{aligned} z &= \omega_0(\zeta) + k_1\delta_1(\zeta,\alpha_1) + k_2\delta_2(\zeta,\alpha_2) + \cdots + k_n\delta_n(\zeta,\alpha_n) \\ &\triangleq \omega_0(\zeta) + \omega_{\text{micro}}(\zeta), \end{aligned} \tag{85}$$

where $k_n = -\mathrm{e}^{-2\mathrm{i}\alpha_n}\omega_0'(\mathrm{e}^{-\mathrm{i}\alpha_n})$.

Figure 2(c) shows an example of the transformation. It indicates that the above transformation could successfully map the complicated domain into a unit disk. In the neighborhood of each defect center, there might be two branch points located on the unit circle. Since the function is not differentiable at the branch point, the transformation is not conformal anymore at the point. These points should not overlap with each other in order to guarantee the accuracy of transformation.

Scale separation for multiple defect problems is similar to that of single micro-defect, except for replacing the expressions related to ω_{micro} with the formula defined in Eq. (85) or (84).

First, $H(\sigma)$ could be written as

$$\frac{\omega(\sigma)}{\overline{\omega'(\sigma)}} = \frac{\omega_0(\sigma)}{\overline{\omega_0'(\sigma)}} + \frac{\overline{\omega_0'(\sigma)}\sum\limits_{i=1}^{n} k_i\delta_i(\sigma,\alpha_i) - \omega_0(\sigma)\sum\limits_{i=1}^{n}\overline{k_i\delta_i'(\sigma,\alpha_i)}}{\overline{\omega_0'(\sigma)} + \sum\limits_{i=1}^{n}\overline{k_i\delta_i'(\sigma,\alpha_i)}}. \tag{86}$$

Substituting it into Eq. (36), we have the separated form of the complex potential $\varphi_0(\zeta)$,

$$\varphi_{0,\text{macro}}(\zeta) + \frac{1}{2\pi\mathrm{i}}\int_\Gamma \frac{\omega_0(\sigma)}{\overline{\omega_0'(\sigma)}}\frac{\overline{\varphi_{0,\text{macro}}'(\sigma)}}{\sigma-\zeta}\mathrm{d}\sigma = \frac{1}{2\pi\mathrm{i}}\int_\Gamma \frac{f_{0,\text{macro}}}{\sigma-\zeta}\mathrm{d}\sigma, \tag{87}$$

$$\begin{aligned} &\varphi_{0,\text{micro}}(\zeta) + \frac{1}{2\pi\mathrm{i}}\int_\Gamma \Big(\frac{\omega_0(\sigma)}{\overline{\omega_0'(\sigma)}} + \Delta_4\Big)\frac{\overline{\varphi_{0,\text{micro}}'(\sigma)}}{\sigma-\zeta}\mathrm{d}\sigma \\ =& \frac{1}{2\pi\mathrm{i}}\int_\Gamma \frac{f_{0,\text{micro}} - \Delta_4\overline{\varphi_{0,\text{macro}}'(\sigma)}}{\sigma-\zeta}\mathrm{d}\sigma, \end{aligned} \tag{88}$$

where Δ_4 is defined as

$$\Delta_4 = \frac{\overline{\omega_0'(\sigma)}\sum\limits_{i=1}^{n} k_i\delta_i(\sigma,\alpha_i) - \omega_0(\sigma)\sum\limits_{i=1}^{n}\overline{k_i\delta_i'(\sigma,\alpha_i)}}{\overline{\omega_0'(\sigma)} + \sum\limits_{i=1}^{n}\overline{k_i\delta_i'(\sigma,\alpha_i)}}. \tag{89}$$

Except for replacing Δ_1 with Δ_4 which takes the multiple defects into account simultaneously, the above equations have the same forms as those of the single micro-defect situation as shown in Eq. (36).

Similarly, the separated form of $\psi(\zeta)$ could also be obtained as follows:

$$\psi_{0,\text{macro}}(\zeta) + \frac{1}{2\pi\mathrm{i}}\int_\Gamma \frac{\overline{\omega_0(\sigma)}}{\omega_0'(\sigma)}\frac{\varphi_{0,\text{macro}}'(\sigma)}{\sigma-\zeta}\mathrm{d}\sigma = \frac{1}{2\pi\mathrm{i}}\int_\Gamma \frac{\overline{f_{0,\text{macro}}}}{\sigma-\zeta}\mathrm{d}\sigma, \tag{90}$$

$$\begin{aligned} &\psi_{0,\text{micro}}(\zeta) + \frac{1}{2\pi\mathrm{i}}\int_\Gamma \Big(\frac{\overline{\omega_0(\sigma)}}{\omega_0'(\sigma)} + \overline{\Delta_4}\Big)\frac{\varphi_{0,\text{micro}}'(\sigma)}{\sigma-\zeta}\mathrm{d}\sigma \\ =& \frac{1}{2\pi\mathrm{i}}\int_\Gamma \frac{\overline{f_{0,\text{micro}}} - \overline{\Delta_4}\,\varphi_{0,\text{macro}}'(\sigma)}{\sigma-\zeta}\mathrm{d}\sigma. \end{aligned} \tag{91}$$

Equations (87)–(91) provide the governing equations of complex potentials for multiple micro-defect problems. As for the stress field, by replacing $k\delta(\sigma,\alpha)$ with $\sum\limits_{i=1}^{n} k_i\delta_i(\sigma,\alpha_i)$, Eqs. (50)–(52) could also be used. Details of the formula are not elaborated here.

4.2 Hierarchical defects: an elliptic hole with multiple semicircular defects

In this subsection, we consider the problem of an infinite plate with an elliptic hole and multiple semicircular defects on its edge. For semicircular micro-defect, the polar angle between the two branch points (see Fig. 3) could be estimated from Eq. (56),

$$\theta_i \approx 4\rho_i, \tag{92}$$

where i denotes the ith micro-defect, and ρ_i could be calculated by Eq. (68). Thus, the polar angle between the neighbored defect centers should satisfy the following requirement to avoid overlapping of branch points:

$$\alpha_{i+1} - \alpha_i > 2(\rho_{i+1} + \rho_i). \tag{93}$$

Assuming that there are n micro-defects on the elliptic hole, the mapping function (see Eq. (85)) turns to be

$$z_0 = \omega_0(\zeta) + \sum_{i=1}^{n} k_i \delta_i(\zeta, \alpha_i, \rho_i), \tag{94}$$

where

$$k_i = R(1 - m\mathrm{e}^{-2\mathrm{i}\alpha_i}).$$

ρ_i could be calculated from the actual defect size r_i via the formula $r_i = |k_i|\,\rho_i$.

Here, we also assume the plate is subject to a uniformly remote force of q parallel to the y-axis, which is the same as that in Subsection 3.2. Using Eqs. (87)–(91), the macro part as well as the micro part of the stress field could be calculated.

As for the macro part, the expressions are the same,

$$\begin{cases} \sigma_\theta^{\mathrm{macro}} + \sigma_\rho^{\mathrm{macro}} = q\,\mathrm{Re}\,\dfrac{(2\mathrm{e}^{2\mathrm{i}\gamma} - m)\zeta^2 - 1}{m\zeta^2 - 1}, \\ \sigma_\theta^{\mathrm{macro}} - \sigma_\rho^{\mathrm{macro}} + 2\mathrm{i}\tau_{\rho\theta} \\ \quad = q\dfrac{(mR_1^4 + \zeta^2)\zeta^2}{R_1^4(m - \zeta^2/R_1^4)(m\zeta^2 - 1)}\Big(2\mathrm{e}^{2\mathrm{i}\gamma} - m + m\dfrac{1 + m\zeta^2 - 2\mathrm{e}^{2\mathrm{i}\gamma}\zeta^2}{m\zeta^2 - 1}\Big) \\ \qquad + \dfrac{q}{R_1^2(m - \zeta^2/R_1^4)}\Big(\mathrm{e}^{-2\mathrm{i}\gamma} - \dfrac{3\mathrm{e}^{2\mathrm{i}\gamma}\zeta^2 + m\mathrm{e}^{2\mathrm{i}\gamma} - m^2 - 1}{m\zeta^2 - 1}\zeta^2 \\ \qquad + \dfrac{\mathrm{e}^{2\mathrm{i}\gamma}\zeta^2 + m\mathrm{e}^{2\mathrm{i}\gamma} - m^2 - 1}{(m\zeta^2 - 1)^2}2m\zeta^4\Big). \end{cases} \tag{95}$$

To make a distinction from the definition of r_i in Eq. (94), we use $R_1 = |\zeta|$ as the notation of radial coordinate in the ζ-plane, making the above formula slightly different from Eq. (76).

The micro part of potentials could be calculated through similar operations described in Subsection 3.2. First, we have

$$\varphi_{0,\mathrm{micro}}(\zeta) = -\frac{q}{2}\sum_{i=1}^{n} k_i \delta_i(\zeta, \alpha_i), \tag{96}$$

$$\begin{aligned} \psi_{0,\mathrm{micro}}(\zeta) = {} & \frac{q}{2}\sum_{i=1}^{n} k_i \delta_i(\zeta, \alpha_i)\mathrm{e}^{-2\mathrm{i}\gamma} - \frac{\omega_0(1/\zeta) + \sum\limits_{i=1}^{n} \overline{k_i}\delta_i(1/\zeta, -\alpha_i)}{\omega_0'(\zeta) + \sum\limits_{i=1}^{n} k_i \delta_i'(\zeta, \alpha_i)}\varphi_{0,\mathrm{micro}}'(\zeta) \\ & - \frac{\omega_0(1/\zeta)\sum\limits_{i=1}^{n} k_i \delta_i'(\zeta, \alpha_i) - \omega_0'(\zeta)\sum\limits_{i=1}^{n} \overline{k_i}\delta_i(1/\zeta, -\alpha_i)}{\omega_0'(\zeta)(\omega_0'(\zeta) + \sum\limits_{i=1}^{n} k_i \delta_i'(\zeta, \alpha_i))}\varphi_{0,\mathrm{macro}}'(\zeta), \end{aligned} \tag{97}$$

where $\varphi_{0,\mathrm{macro}}(\zeta)$ is the same as Eq. (73),

$$\varphi_{0,\mathrm{macro}}(\zeta) = -\frac{q}{2}R(m - \mathrm{e}^{2\mathrm{i}\gamma})\zeta.$$

Thus, we have

$$\psi_{\mathrm{micro}}(\zeta) = -\frac{q}{2}\mathrm{e}^{-2\mathrm{i}\gamma}\sum_{i=1}^{n} k_i\delta_i(\zeta,\alpha_i) + \psi_{0,\mathrm{micro}}(\zeta). \tag{98}$$

Finally, we can obtain

$$\sigma_\theta^{\mathrm{micro}} + \sigma_\rho^{\mathrm{micro}} = 4\,\mathrm{Re}\left(\frac{\omega_0'(\zeta)\varphi_{\mathrm{micro}}'(\zeta) - \sum\limits_{i=1}^{n} k_i\delta_i'(\zeta,\alpha_i)\varphi_{\mathrm{macro}}'(\zeta)}{\omega_0'(\zeta)\Big(\omega_0'(\zeta) + \sum\limits_{i=1}^{n} k_i\delta_i'(\zeta,\alpha_i)\Big)}\right), \tag{99}$$

and

$$\begin{aligned}\sigma_\theta^{\mathrm{micro}} - \sigma_\rho^{\mathrm{micro}} + 2\mathrm{i}\tau_{\rho\theta}^{\mathrm{micro}} = {} & \frac{2\zeta}{\overline{\zeta}\Big(\overline{\omega_0'(\zeta)} + \overline{\sum\limits_{i=1}^{n} k_i\delta_i'(\zeta,\alpha_i)}\Big)}\Delta_5 - \frac{2\zeta\overline{\sum\limits_{i=1}^{n} k_i\delta_i'(\zeta,\alpha_i)}}{\overline{\zeta}\,\overline{\omega_0'(\zeta)}\Big(\overline{\omega_0'(\zeta)} + \overline{\sum\limits_{i=1}^{n} k_i\delta_i'(\zeta,\alpha_i)}\Big)} \\ & \cdot (\overline{\omega_0(\zeta)}\Phi_{\mathrm{macro}}'(\zeta) + \omega_0'(\zeta)\Psi_{\mathrm{macro}}(\zeta)),\end{aligned} \tag{100}$$

where Δ_5 is defined as

$$\begin{aligned}\Delta_5 = {} & \overline{\omega_0(\zeta)}\Phi_{\mathrm{micro}}'(\zeta) + \overline{\sum_{i=1}^{n} k_i\delta_i(\zeta,\alpha_i)}\Phi_{\mathrm{macro}}'(\zeta) + \overline{\sum_{i=1}^{n} k_i\delta_i(\zeta,\alpha_i)}\Phi_{\mathrm{micro}}'(\zeta) \\ & + \omega_0'(\zeta)\Psi_{\mathrm{micro}}(\zeta) + \sum_{i=1}^{n} k_i\delta_i'(\zeta,\alpha_i)\Psi_{\mathrm{macro}}(\zeta) + \sum_{i=1}^{n} k_i\delta_i'(\zeta,\alpha_i)\Psi_{\mathrm{micro}}(\zeta).\end{aligned} \tag{101}$$

As an example, we calculate a dual micro-defects problem with $\alpha_1 = 0$ (i.e., $\beta = 0°$), $\rho_1 = 0.1\,\mathrm{mm}$, $\alpha_2 = \pi/4$ (i.e., $\beta = 18.4°$), and $\rho_2 = 0.01\,\mathrm{mm}$. Other parameters are $a = 3\,\mathrm{mm}$, $b = 1\,\mathrm{mm}$, $\gamma = \pi/2$, and $q = 1\,\mathrm{MPa}$. The circumferential stress along the hole edge is plotted in Fig. 9. It shows that the micro part of σ_θ oscillates in the neighborhood of $\alpha = 0°$ and $20°$, and rapidly approaches zero afar. The curve has two stress peaks, which correspond to the locations of the two micro-defects, respectively.

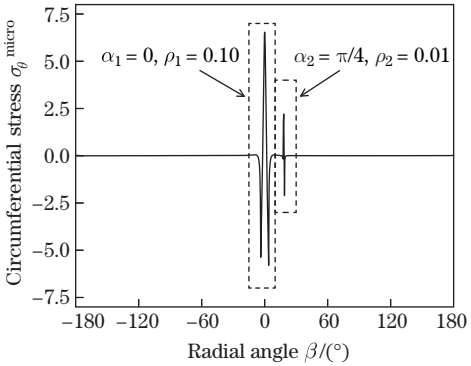

Fig. 9 Area of influence for multiple micro-defects

The interactive effect between multiple edge defects is also investigated. Let the first micro-defect at $\beta = 0°$ with $r = 0.1\,\text{mm}$ be fixed. The location and size of the second micro-defect vary. In this case, $a = 3\,\text{m}$, $b = 2\,\text{mm}$, $\gamma = \pi/2$, and $q = 1\,\text{MPa}$. The stress concentrations at the front tip of the first defect K_{micro} are shown in Fig. 10.

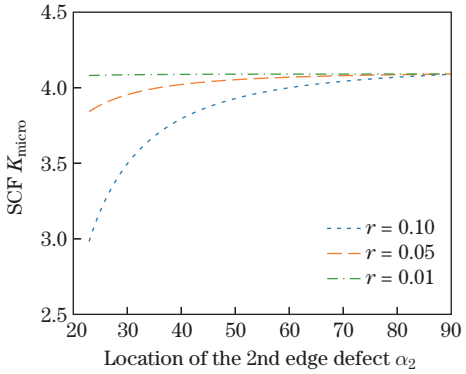

Fig. 10 Interaction effect of multiple edge defects (color online)

It could be seen that the multiple micro-defects have an interactive effect on the stress field, especially when the distance is close. However, if the distance is large enough, the interaction could be ignored as all curves retreat to its original SCF value caused solely by the first micro-defect (here approximately at 4.1). Generally, the coalescence of micro-defects may release the stress concentration, which is understandable if noticing that a smaller radius of micro-defect leads to a higher stress concentration in the previous section. It can also be seen from Fig. 10 that a larger radius of the second defect has a greater effect on the first defect, and certainly has a larger area of influence. An extreme case is that when the size of the second crack is 0.01 mm, its effect is negligible.

5 Conclusions

A multiscale framework for the analytical solution of the stress field of hierarchical defects is formulated. Emphasis is laid on the hierarchical defects at different scales. Within the general multiscale framework, this mathematical model can be flexibly applied to a variety of engineering problems. The accurate analytical solution is also capable of capturing the factors that significantly affect the process of crack propagation. The main findings are summarized as follows:

(i) Representation of the conformal mapping, the governing equations of potentials, and the stress field at two scales is analytically achieved within the formulated multiscale framework.

(ii) The influence of the secondary micro-defect is local but cannot be ignored under certain circumstances. The present work provides a general tool to exactly investigate the influence. A modified formula $K_{\text{u}} = 1 + 2K_0$ is proposed to estimate the stress concentrations.

(iii) One of the benefits of the multi-scale framework is to solve the problems of multiple edge defects. The results show that multiple micro-defects have an interactive effect on the stress filed. Coalescence of micro-defects may release the stress concentration.

The proposed framework can be extended to more general problems, such as primary defect modeled as a square hole or a blunt crack, secondary defect modeled as a micro edge crack, even solution of three levels of hierarchical defects is feasible. Nevertheless, it shall be noted that the formulated multiscale framework is stipulated to elastic materials. Last but not least, the approach can be also applied to additive manufacturing materials, bio-inspired materials that have the features of hierarchical defects[29–31]. They are left for our forthcoming work.

References

[1] ARAVAS, N. and MCMEEKING, R. Finite element analysis of void growth near a blunting crack tip. *Journal of the Mechanics and Physics of Solids*, **33**(1), 25–49 (1985)

[2] ARAVAS, N. and MCMEEKING, R. Microvoid growth and failure in the ligament between a hole and a blunt crack tip. *International Journal of Fracture*, **29**(1), 21–38 (1985)

[3] UNGER, D. J. Linear elastic solutions for slotted plates. *Journal of Elasticity*, **108**(1), 67–82 (2012)

[4] HUANG, Z. Y. and KUANG, Z. B. A first order perturbation analysis of a non-ideal crack in a piezoelectric material. *International Journal of Solids and Structures*, **38**(40/41), 7261–7281 (2001)

[5] MUSKHELISHVILI, N. I. *Some Basic Problems of the Mathematical Theory of Elasticity*, Springer Science & Business Media, Berlin (2013)

[6] ENGLAND, A. H. *Complex Variable Methods in Elasticity*, Dover Publications, Inc., New York (2003)

[7] BELYTSCHKO, T. and BLACK, T. Elastic crack growth in finite elements with minimal remeshing. *International Journal for Numerical Methods in Engineering*, **45**(5), 601–620 (1999)

[8] WU, B. J. and TANG, K. Modelling on crack propagation behaviours at concrete matrix-aggregate interface. *Fatigue & Fracture of Engineering Materials & Structures*, **42**(8), 1803–1814 (2019)

[9] KNIGHT, M., WROBEL, L., and HENSHALL, J. Fracture response of fibre-reinforced materials with macro/microcrack damage using the boundary element technique. *International Journal of Fracture*, **121**(3/4), 163–182 (2003)

[10] SUN, F., DONG, C., and YANG, H. Isogeometric boundary element method for crack propagation based on Bézier extraction of NURBS. *Engineering Analysis with Boundary Elements*, **99**, 76–88 (2019)

[11] ZAPPALORTO, M., SALVIATO, M., and MARAGONI, L. Analytical study on the mode III stress fields due to blunt notches with cracks. *Fatigue & Fracture of Engineering Materials & Structures*, **42**(3), 612–626 (2019)

[12] GOOGARCHIN, H. S. and MOAZZEZ, K. Analytical solution for free vibration of cracked orthotropic cylindrical shells. *International Journal of Mechanical Sciences*, **153**, 254–270 (2019)

[13] HUANG, X., LIU, Y., and HUANG, X. Analytical characterizations of crack tip plastic zone size for central-cracked unstiffened and stiffened plates under biaxial loading. *Engineering Fracture Mechanics*, **206**, 1–20 (2019)

[14] LAZZARIN, P., BERTO, F., and RADAJ, D. Fatigue-relevant stress field parameters of welded lap joints: pointed slit tip compared with keyhole notch. *Fatigue & Fracture of Engineering Materials & Structures*, **32**(9), 713–735 (2009)

[15] BERTO, F. and LAZZARIN, P. Multiparametric full-field representations of the in-plane stress fields ahead of cracked components under mixed mode loading. *International Journal of Fatigue*, **46**, 16–26 (2013)

[16] SIH, G. and TANG, X. S. Dual scaling damage model associated with weak singularity for macroscopic crack possessing a micro/mesoscopic notch tip. *Theoretical and Applied Fracture Mechanics*, **42**(1), 1–24 (2004)

[17] FANG, Q. H., SONG, H. P., and LIU, Y. W. Elastic behaviour of an edge dislocation near a sharp crack emanating from a semi-elliptical blunt crack. *Chinese Physics B*, **19**(1), 016102 (2010)

[18] HE, T. W. and FENG, M. L. Influence of nanoscale deformation twins near a slant edge crack tip on crack blunting in nanocrystalline metals. *Engineering Fracture Mechanics*, **184**, 286–295 (2017)

[19] YU, M., FANG, Q. H., FENG, H., and LIU, Y. W. Effect of special rotational deformation on dislocation emission from interface collinear crack tip in nanocrystalline bi-materials. *Acta Mechanica*, **227**(7), 2011–2024 (2016)

[20] TORABI, A., BAHRAMI, B., and AYATOLLAHI, M. On the use of digital image correlation method for determining the stress field at blunt V-notch neighborhood. *Engineering Fracture Mechanics*, **223**, 106768 (2020)

[21] BAHRAMI, B., AYATOLLAHI, M., and TORABI, A. Application of digital image correlation method for determination of mixed mode stress intensity factors in sharp notches. *Optics and Lasers in Engineering*, **124**, 105830 (2020)

[22] SIH, G. and TANG, X. Triple scale segmentation of non-equilibrium system simulated by macro-micro-atomic line model with mesoscopic transitions. *Theoretical and Applied Fracture Mechanics*, **44**(2), 116–145 (2005)

[23] TANG, X. and SIH, G. Weak and strong singularities reflecting multiscale damage: micro-boundary conditions for free-free, fixed-fixed and free-fixed constraints. *Theoretical and Applied Fracture Mechanics*, **43**(1), 5–62 (2005)

[24] TANG, K. and LI, S. Interactive creep-fatigue crack growth of 2024-T3 Al sheets: selective transitional functions. *Fatigue & Fracture of Engineering Materials & Structures*, **38**(5), 597–609 (2015)

[25] TANG, K., BERTO, F., and WU, H. Fatigue crack growth in the micro to large scale of 7075-T6 Al sheets at different R ratios. *Theoretical and Applied Fracture Mechanics*, **83**, 93–104 (2016)

[26] TANG, K., WANG, Z., and BERTO, F. Time-temperature effects in dual scale crack growth of titanium alloys. *Theoretical and Applied Fracture Mechanics*, **97**, 368–375 (2018)

[27] TIMOSHENKO, S. P. and GOODIER, J. N. *Theory of Elasticity*, McGraw Hill, New York (1970)

[28] INGLIS, C. E. Stresses in a plate due to the presence of cracks and sharp corners. *Transactions of the Institute of Naval Architects*, **55**, 219–241 (1913)

[29] SHIN, Y. A., YIN, S., LI, X., LEE, S., MOON, S., JEONG, J., and OH, S. H. Nanotwin-governed toughening mechanism in hierarchically structured biological materials. *Nature Communications*, **7**(1), 10772 (2016)

[30] MIRZAEIFAR, R., DIMAS, L. S., QIN, Z., and BUEHLER, M. J. Defect-tolerant bioinspired hierarchical composites: simulation and experiment. *Acs Biomaterials Science & Engineering*, **1**(5), 295–304 (2015)

[31] BELL, D. and SIEGMUND, T. 3D-printed polymers exhibit a strength size effect. *Additive Manufacturing*, **21**, 658–665 (2018)

Appendix A

A plate with a hole of unit circle and a micro semicircular defect at $z = 1$, as shown in Fig. A1 (the z-plane). Assuming that the radius of the defect is ρ, the mapping function could be constructed through the process below.

First, a fractional linear transformation $f_2(z)$ could transform the domain into a domain in the upper plane as shown in the z_2-plane in the figure.

$$z_2 = f_2(z) = \mathrm{i}\frac{1-\frac{1}{z}}{1+\frac{1}{z}} = \mathrm{i}\frac{z-1}{z+1}. \tag{A1}$$

In the transformation, the intersection points between the unit circle and the micro-defect are mapped to $z_2 = -\frac{\rho}{2}$ and $z_2 = \frac{\rho}{2}$.

Now, another fractional linear transformation $f_3(z_2)$ is introduced to map the domain in the z_2-plane onto the whole upper plane, as described in the z_3-plane. The function maps the point $z_2 = -\frac{\rho}{2}$ to be $z_3 = 0$, the point $z_2 = \frac{\rho}{2}\mathrm{i}$ to be $z_3 = 1$, and the point $z_2 = \frac{\rho}{2}$ to be ∞.

$$z_3 = f_3(z_2) = -\Big(\frac{z_2+\frac{\rho}{2}}{z_2-\frac{\rho}{2}}\Big)^2. \tag{A2}$$

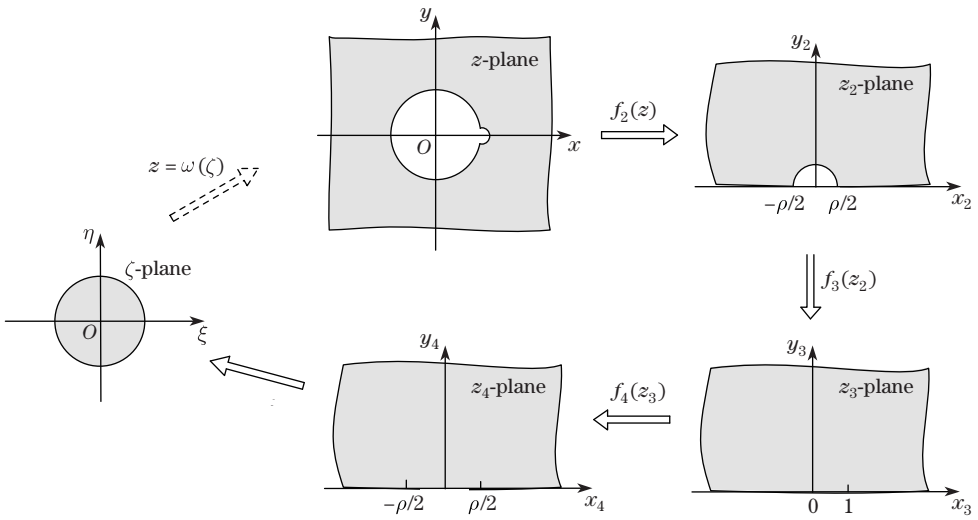

Fig. A1 Conformal mapping

Once again, a fractional linear transformation is constructed, aiming to map $z_3 = 0$, $z_3 = \infty$, and $z_3 = 1$ to be $z_4 = -\frac{\rho}{2}$, $z_4 = \frac{\rho}{2}$, and the origin $z_4 = 0$, respectively. Assuming that it has the form of

$$z_4 = f_4(z_3) = \frac{kz_3 + m}{n + z_3}, \tag{A3}$$

the parameters of k, m, and n could be determined by satisfying the above mapping requirements, yielding

$$z_4 = f_4(z_3) = \frac{\rho}{2}\frac{z_3 - 1}{1 + z_3}. \tag{A4}$$

The above transformation does not change the shape of the domain, it just constructed for maps several special points to required positions. Through Eqs. (A2) and (A3), the point of $-\frac{\rho}{2}$, $\frac{\rho}{2}$, and $\frac{\rho}{2}\mathrm{i}$ in the z_2-plane are mapped to be $-\frac{\rho}{2}$, $\frac{\rho}{2}$, and 0 in the z_4-plane.

In order to map the upper plane onto the unit disk, use the following transformation:

$$z_5 = \frac{\mathrm{i} - z_4}{\mathrm{i} + z_4}. \tag{A5}$$

It is found that the center of unit disk in z_5 is mapped not from ∞ but $\zeta_0 = -\frac{4+\rho^2}{-12+\rho^2}$ (in the z-plane). Therefore, we introduce the transformation

$$\zeta = \frac{z_5 - \zeta_0}{1 - \overline{\zeta_0} z_5}. \tag{A6}$$

Through Eqs. (A1)–(A5), the domain of an infinite plate with a circular hole and a semicircular edge defect is successfully mapped onto a unit disk.